J Artif Organs (2011) 14:215–222
DOI 10.1007/s10047-011-0568-6

ORIGINAL ARTICLE

Efficient transfection method using deacylated polyethylenimine-coated magnetic nanoparticles

Daisuke Kami · Shogo Takeda · Hatsune Makino · Masashi Toyoda · Yoko Itakura · Satoshi Gojo · Shunei Kyo · Akihiro Umezawa · Masatoshi Watanabe

Received: 6 October 2010 / Accepted: 31 March 2011 / Published online: 3 May 2011

Abstract Low efficiencies of nonviral gene vectors, such as transfection reagent, limit their utility in gene therapy. To overcome this disadvantage, we report on the preparation and properties of magnetic nanoparticles [diameter (d) = 121.32 ± 27.36 nm] positively charged by cationic polymer deacylated polyethylenimine (PEI max), which boosts gene delivery efficiency compare with polyethylenimine (PEI), and their use for the forced expression of plasmid delivery by application of a magnetic field. Magnetic nanoparticles were coated with PEI max, which enabled their electrostatic interaction with negatively charged molecules such as plasmid. We successfully transfected 81.1 ± 4.0% of the cells using PEI max-coated magnetic nanoparticles (PEI max-nanoparticles). Along with their superior properties as a DNA delivery vehicle, PEI max-nanoparticles offer to deliver various DNA formulations in addition to traditional methods. Furthermore, efficiency of the gene transfer was not inhibited in the presence of serum in the cells. PEI max-nanoparticles may be a promising gene carrier that has high transfection efficiency as well as low cytotoxicity.

Keywords Deacylated polyethylenimine · Magnetic nanoparticle · Efficient nonviral transfection method

D. Kami
Innovative Integration between Medicine and Engineering Based on Information Communications Technology, Yokohama National University Global COE Program, Yokohama, Japan
e-mail: dkami@tmig.or.jp

S. Takeda · M. Watanabe (✉)
Laboratory for Medical Engineering, Division of Materials and Chemical Engineering, Yokohama National University, 79-1 Tokiwadai, Hodogaya-ku, Yokohama 240-8501, Japan
e-mail: mawata@ynu.ac.jp

D. Kami · H. Makino · M. Toyoda · A. Umezawa
Department of Reproductive Biology, National Institute for Child Health and Development, Tokyo, Japan

D. Kami · M. Toyoda (✉) · Y. Itakura · S. Gojo
Vascular Medicine, Research Team for Geriatric Medicine, Tokyo Metropolitan Institute of Gerontology, 35-2 Sakae-cho, Itabashi-ku, Tokyo 173-0015, Japan
e-mail: mtoyoda@tmig.or.jp

S. Gojo · S. Kyo
Division of Therapeutic Strategy for Heart Failure, Department of Cardio-Thoracic Surgery, The University of Tokyo, Tokyo, Japan

Introduction

Nanotechnologies that allow the nondisruptive introduction of carriers in vivo have wide potential for gene and therapeutic delivery systems [1–4]. Extremely small particles have been successfully introduced into living cells without any further modification to enhance endocytic internalization, such as for cationic help. The cells containing the internalized nanoparticles continued to thrive, indicating that the particles have no inhibitory effect on mitosis. Therefore, iron oxide magnetic nanoparticles have played an important role as magnetic resonance imaging contrast agents [5, 6], and cytotoxicity of this nanoparticle was none (or low) [7, 8]. Thereby, the functionalized iron oxide magnetic nanoparticles are expected to be useful as a new gene delivery tool [3].

Cationic polymer polyethylenimine (PEI) (linear, MW 25,000) is known as the transfection reagent in molecular biology [9], and the dispersant in nanotechnology [10]. PEI are configured to form the positively charged complex with DNA, which binds to anionic cell surface residues and

enter the cell via endocytosis [9, 11], keeping the dispersed state in the solution [10]. However, PEI containing residual *N*-acyl groups is a disadvantage for transfection efficiency. Also, the deacylated PEI (PEI max) for transfection reagent was reported, showing an increase in optimal transfection efficiency of 21-fold in comparison with PEI [12].

The transfection method using magnetic nanoparticles utilizes a magnetic force to deliver DNA into target cells. Therefore, the plasmid is first associated with magnetic nanoparticles. Then, the application of a magnetic force drives the plasmid–nanoparticle complexes toward and into the target cells, where the cargo is released (Fig. 1a) [13–16]. The magnetic nanoparticles are also coated with biological polymers, such as PEI, to allow plasmid loading (Fig. 1b). The binding of the negatively charged plasmid to the positively charged PEI max-coated magnetic nanoparticles (PEI max-nanoparticles) occurs relatively quickly. After complex formation, the loaded nanoparticles are incubated together with the target cells on a magnet plate. Owing to the magnetic force, the iron particles are rapidly drawn toward the surface of the cell membrane. Cellular uptake occurs by either endocytosis or pinocytosis [17]. Once delivered to the target cells, the plasmid is released into the cytoplasm [17, 18]. The magnetic nanoparticles accumulate in endosomes and/or vacuoles [18]. Over time, the nanoparticles are degraded and the iron enters normal iron metabolism [19]. An influence of magnetic nanoparticles on cellular functions has not been reported yet. However, in most cases, the increased iron concentration in culture media does not lead to cytotoxic effects [7].

In this study, we coated the transfection reagent, PEI max, on the surface of magnetic nanoparticles and applied a gene vector using PEI max-nanoparticles for a highly efficient transfection method. Our results indicate a high level of expression of the transfected gene in living cells using the plasmid-conjugated PEI max-nanoparticles.

Materials and methods

Materials

Magnetic nanoparticles (γ-Fe_2O_3, $d = 70$ nm) were purchased from CIK NanoTek. PEI max linear (MW 25,000) was purchased from Polysciences Inc. FuGENE HD was purchased from Roche Diagnostics. Deionized water was purchased from Gibco. Magnetic sheet (160 mT), and neodymium magnet (130 mT) was purchased from Magna Co. Ltd.

Preparation of the PEI max-nanoparticles

The magnetic nanoparticles (1.0 g) were dissolved in 30 ml of PEI max solution (1.6 mg PEI max/ml). The mixture was sonicated for 2 min (40 W) on ice, and 20 ml of deionized water was added (final concentration 1.0 mg PEI max/ml). The ferrofluid was centrifuged at 4,100×*g* for 5 min. The supernatant fluids were harvested and transferred into a fresh tube. This fluid was washed twice by deionized water and resolved into an equal volume of the PEI max solution (1.0 mg PEI max/ml). Magnetic nanoparticles in this fluid

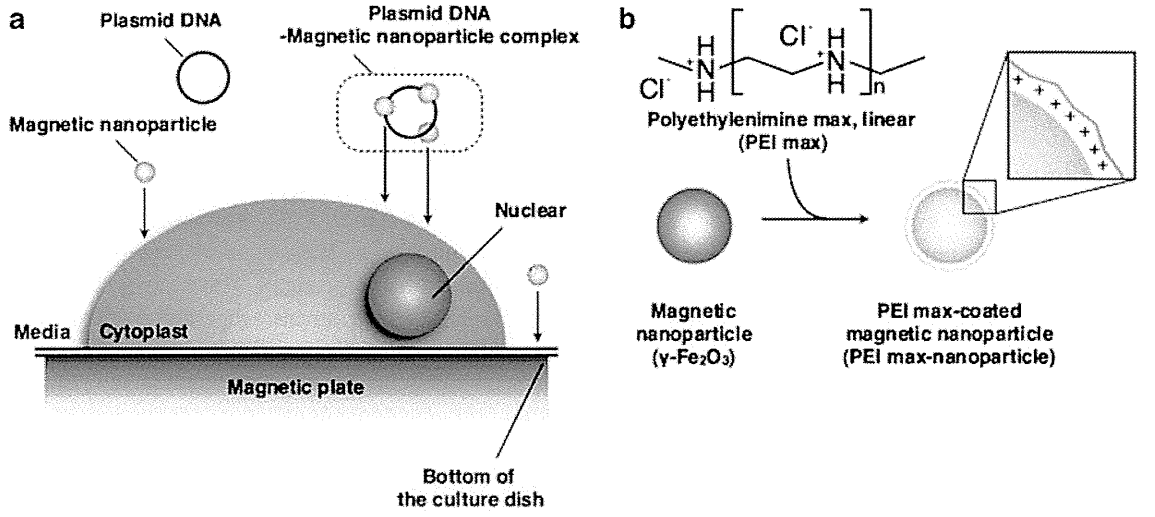

Fig. 1 Nanoparticle transfection method and cationic coating: **a** Plasmid-conjugated magnetic nanoparticles moved to the cell surface on the magnetic sheet upon application of magnetic force. Then, the magnetic force drove this complex toward and into the target cells. **b** Magnetic nanoparticles (γ-Fe_2O_3, $d = 70$ nm) (CIK NanoTek Inc.) were coated with deacylated polyethylenimine max linear (PEI max) (MW 25,000) (Polysciences Inc.), known as a dispersive agent, and transfection reagents. The surface of the PEI max-nanoparticle was positively charged. Nanoparticles and plasmid formed complexes by ionic interaction of the negatively charged plasmid and the positively charged surface of the PEI max-nanoparticle

were coated with PEI max and dispersed in PEI max solution or deionized water.

Measurement of PEI max-nanoparticle size and ζ-potential

The size of the PEI max-nanoparticles was measured with a laser light-scattering method using a fiberoptics particle analyzer (FPAR-1000, Otsuka Electronics). The measurement was performed in triplicate, and median size and range of size distribution were obtained. The ζ-potential of the PEI max-nanoparticles was determined with electrophoretic light-scattering spectrophotometer (ELSZ-2, Otsuka Electronics).

Charge characteristics of PEI max-nanoparticle

PEI max-nanoparticle (100 μg) and each weight of plasmid (2,000, 1,000, 750, 500, 375, 250, 188 ng) were mixed in deionized water or PEI max solution (1 mg/ml). Each solution were reacted for 1 h at room temperature.

Plasmid DNA was bound to PEI max-nanoparticles

Plasmid DNA (5 μg) was reacted with various weights of PEI max-nanoparticles (0–1.8 mg/tube) in deionized water for 15 min at room temperature. Then, the reaction mixtures were centrifuged at 12,000×*g* for 15 min and were formed in a sol-like precipitation in the lower layer. The concentration of DNA in the upper layer (hyaline layer) was determined by NanoDrop 1000 spectrophotometer (Thermo Scientific). The relative concentration of plasmid DNA treated without PEI max-nanoparticles was regarded as 100%.

Cell culture

P19CL6 cells (CL6 cells) from a mouse embryonic carcinoma cell line were grown on 100-mm dishes (Becton-Dickinson) in alpha-minimum essentioal medium (MEM) (Nacalai Tesque) supplemented with 10% fetal bovine serum (FBS) (JRH Bioscience Inc.), penicillin, and streptomycin (Gibco), and were maintained in a 5% carbon dioxide (CO_2) atmosphere at 37°C.

Transfection procedure using PEI max-nanoparticles

CL6 cells were seeded at 1×10^5 cells/well in six-well plates (Becton-Dickinson) 18 h before transfection. Immediately before transfection, cells were rinsed and supplemented with fresh culture medium (1 ml). The PEI max-nanoparticles (in 1 mg PEI max/ml solution) were mixed with 2.0 μg of the plasmid [pCAGGS–enhanced green fluorescent protein (EGFP), the modified pCAGGS expression vector [20], weight ratio PEI max:plasmid = 3:1] and incubated in the deionized water at final volume of 50 μl at room temperature for 15 min. The complexes were added to the CL6 cells on a magnetic sheet various times (0, 0.5, 1, 4, and 24 h). Forty-eight hours after transfection, CL6 cells were evaluated; 1 mg/ml of PEI max solution was used as a positive control.

Quantitative real-time reverse transcriptional (RT)-PCR

Total RNAs from CL6 cells were extracted using ISOGEN (Nippon Gene). To perform quantitative real-time polymerase chain reaction (PCR) assay, total RNA (1 μg) was reverse-transcribed using random hexamer and the PrimeScript RT reagent kit (TaKaRa). Quantitative real-time reverse transcriptional (RT)-PCR was performed on LineGene (BioFlux), using 100 ng of complementary DNA (cDNA) in 25 μl reaction volumes with 10 nmol/l EGFP primer and 12.5 μl of SYBR Premix Ex Taq (TaKaRa). PCR primers for the gene of EGFP and *Gapdh* were designed to amplify each cDNA using the sense primer (5′-CCGACCACATGAAGCAGCAC-3′) and the reverse primer (5′-CTTCAGCTCGATGCGGTTCAC-3′) for the EGFP, and the sense primer (5′-TGCGACTTCAACAGCA ACTC-3′) and the reverse primer (5′-CTTGCTCAGTGTC CTTGCTG-3′) for the *Gapdh*. Calculations were automatically performed by fluorescent quantitative detection system software (BioFlux).

Nanoparticle cytotoxicity

Alamar Blue [21] was used to measure cell proliferation and metabolic activity as an oxidation-reduction indicator. After 48 h of PEI max or PEI max-nanoparticle exposure, 900 μl of medium from each condition was transferred into a 24-well flat-bottomed plate. One hundred microliters of Alamar Blue (AbD Serotec) was added to each well, and the well plate was incubated for 3 h at 37°C. Fluorescence was measured at 570/600 nm in a Viento multispectrophotometer reader (Dainippon Pharmaceutical). The relative absorbance of CL6 cells without any treatment is regarded as 100% (it is indicated as a percent control in Fig. 4c).

Flow cytometric analysis

To count the numbers of EGFP-positive cells using PEI max-nanoparticles (0.8 μg/well in a six-well plate) on a magnetic sheet for 4 h (PEI max alone as a positive control), a Cytomics FC500 (Beckman Coulter Inc.) was used, and data were analyzed with FlowJo Ver.7 (Tree Star Inc.). Each sample was compared with negative control cells (without treatment).

Statistical analysis

Results, shown as the mean ± standard error (SE), were compared by analysis of variance (ANOVA) followed by Scheffe test (http://chiryo.phar.nagoya-cu.ac.jp/javastat/JavaStat-j.htm), with $P < 0.05$ considered significant.

Results

Characterization of PEI max-nanoparticles

Magnetic nanoparticles were well coated with PEI max and were highly dispersed in PEI max solution (1 mg/ml) or deionized water. Secondary size of the PEI max-nanoparticles was approximately 121.32 ± 27.36 nm (Fig. 2A). To evaluate stability in PEI max solution (1 mg/ml) or deionized water, we measured the ζ-potential of PEI max-nanoparticles, which was +45.53 mV in PEI max solution and +30.05 mV in deionized water. The PEI max-nanoparticles were aggregated by magnetic force (Fig. 2Ba) and quickly redispersed by vortex (Fig. 2Bb). Time-lapse photography (30 s/s) shows that magnetic nanoparticles were gradually removed at the site of the neodymium magnet (right side of the tube) for 2 h (magnetic nanoparticles for transfection: http://www.youtube.com/watch?v=Hyjfc4moHK4). These nanoparticles in PEI max solution were not aggregated without magnetic force. To avoid aggregation of plasmid-attached PEI max-nanoparticle caused by charge neutralization, it was necessary that their weight ratio was approximately 1:400 (Fig. 2C). In general, 1–2 μg of plasmid per well was mixed with the transfection reagent such, as PEI max, and FuGENE HD into six-well plates. However, too much (400–800 μg of nanoparticle per well) caused inhibition of transfection (described later). To solve the problem, we decided to use in 1 mg/ml of PEI max solution as a solvent. As a result, each concentration of the plasmid did not aggregate with PEI max-nanoparticle (Fig. 2Bb). To evaluate whether the plasmid DNA was attached to PEI max-nanoparticles in deionized water, we reacted PEI max-nanoparticles with plasmid DNA for 15 min at room temperature. Measuring the concentration of plasmid DNA in the upper layer (hyaline layer), the weight of PEI max-nanoparticles was reduced in a dependent manner (Fig. 2D).

Transfection efficiency using PEI max-nanoparticles and magnetic sheet, and viability of the CL6 cells treated with PEI max-nanoparticles

CL6 cells were transfected with pCAGGS-EGFP and PEI max alone as a positive control (Fig. 3a) and pCAGGS-EGFP and PEI max-nanoparticles (Fig. 3b) at 48 h after transfection. Many EGFP-positive cells were observed among CL6 cells transfected with PEI max-nanoparticles compared with those transfected with PEI max. To evaluate the optimum condition of transfection using PEI max-nanoparticles, quantitative real-time RT-PCR was performed at 48 h after transfection. The optimum condition of transfection was a concentration of 0.8 μg/well (Fig. 4a) on a magnetic sheet for 4 h (Fig. 4b). *EGFP* gene expression level was reduced under transfection of excess magnetic nanoparticles (7.5 μg/well) (Fig. 4a) and prolonged time on the magnetic sheet (24 h) (Fig. 4b). EGFP expression in CL6 cells transfected with PEI max-nanoparticles was increased approximately two to fourfold compared with those transfected with PEI max. The viability of CL6 cells treated with PEI max-nanoparticles, as measured by Alamar Blue assay, did not differ between cells treated with/without PEI max alone (Fig. 4c).

Number of EGFP-positive cells by flow cytometric analysis

Forty-eight hours after transfection using PEI max alone or PEI max-nanoparticles, we examined the number of EGFP-positive cells (total 10,000 cells) by flow cytometric analysis. Compared with the negative control (untreated CL6 cells), 42.2 ± 8.5% of cells treated with PEI max alone (Fig. 5a), 81.1 ± 4.0% of cells treated with 0.8 μg of PEI max-nanoparticles per well on the magnetic sheet for 4 h (Fig. 5b), and 13.9 ± 1.1% of cells treated with FuGENE HD (Fig. 5c) expressed EGFP. The number of EGFP-positive cells was significantly increased (approximately twofold) using PEI max-nanoparticles.

Discussion

In this study, to express target gene with high efficiency and low cytotoxicity, we focused on PEI max and magnetic nanoparticles (γ-Fe_2O_3). Many researchers have reported various transfection methods using PEI and magnetic nanoparticles, such as γ-Fe_2O_3, and superparamagnetic iron oxide nanoparticle (used as magnetic resonance imaging contrast agents) (Table 1). However, these methods had a low transfection efficiency [14, 15], combined with virus (adenovirus, or retrovirus) [15], and high cytotoxicity (low cell viability) [13] and may therefore have little effectiveness for clinical use.

The expression level of the *EGFP* gene was reduced under transfection of excess magnetic nanoparticles (7.5 μg/well) (Fig. 4a). This result may indicate that a high concentration of PEI max-nanoparticles formed the large agglutinate complexes with plasmid DNAs [22, 23]

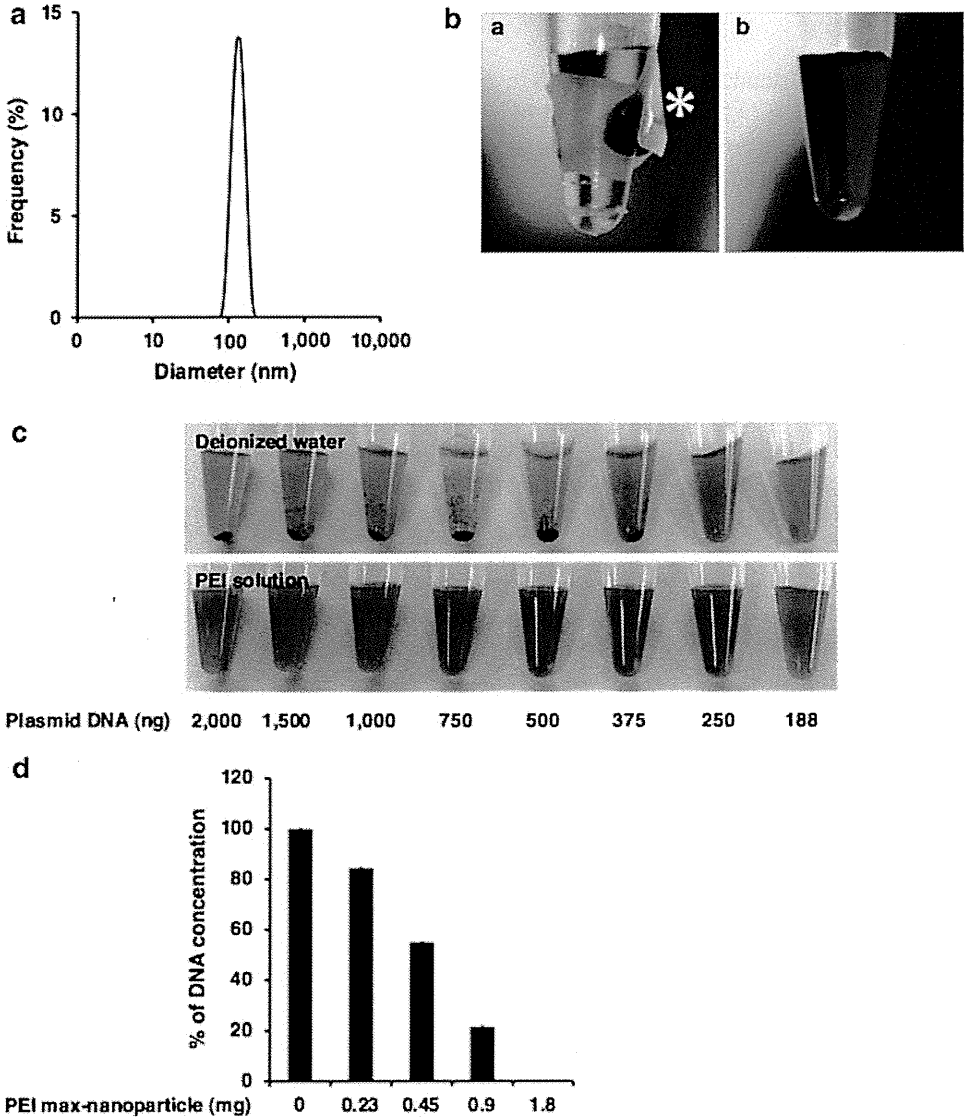

Fig. 2 Characteristics of the deacylated polyethylenimine (PEI max)-nanoparticle: **a** The size of the PEI max-nanoparticles was measured with a laser light-scattering method using a fiberoptics particle analyzer (FPAR-1000, Otsuka Electronics) at 37°C. Secondary particle size of the PEI max-nanoparticles was approximately 121.32 ± 27.36 nm. **b** PEI max-nanoparticles were induced to aggregate by a magnet (*a*) and were then dispersed (*b*). *Asterisk* indicates column-shaped neodymium magnet. **c** Cationic PEI max-nanoparticles (100 μg per tube) in deionized water or PEI max solution (1 mg/ml) were reacted with anionic plasmid [pCAGGS–enhanced green fluorescent protein (EGFP)] by an ionic bond. PEI max-nanoparticles in deionized water and plasmid aggregated more easily than that in PEI max solution and plasmid. **d** To evaluate whether plasmid DNA attached to PEI max-nanoparticles in deionized water, PEI max-nanoparticles were reacted with plasmid DNA for 15 min at room temperature. Measuring the concentration of plasmid DNA in the upper layer (hyaline layer), the weight of PEI max-nanoparticles was reduced in a dependent manner

because PEI max-nanoparticle and plasmid DNA complexes are taken in by endocytosis. Thus, it might be difficult to take the large complexes into the cytoplasm by endocytosis. Furthermore, the expression level of the *EGFP* gene was also reduced under transfection during a prolonged time on the magnetic sheet (24 h) (Fig. 4b). This result may demonstrate a causal relationship between the cell division cycle and time on the magnetic sheet. Plasmid DNAs in the cytoplasm were transported into the nucleus when the nuclear membrane disappeared on cell division [24]. Thus, plasmid DNAs and magnetic nanoparticle complexes might not be transported into the nucleus because they are drawn to the bottom of the cell by magnetic force.

We succeeded in producing PEI max-nanoparticles that enabled P19CL6 cells, which is derived from embryonic carcinoma transfected on a magnetic sheet. In addition, this method resulted in a highly efficient gene transduction compared with that of conventional transfection methods (Fig. 5a, c). This transfection method using PEI max-nanoparticles is a relatively low-cost and quick method of

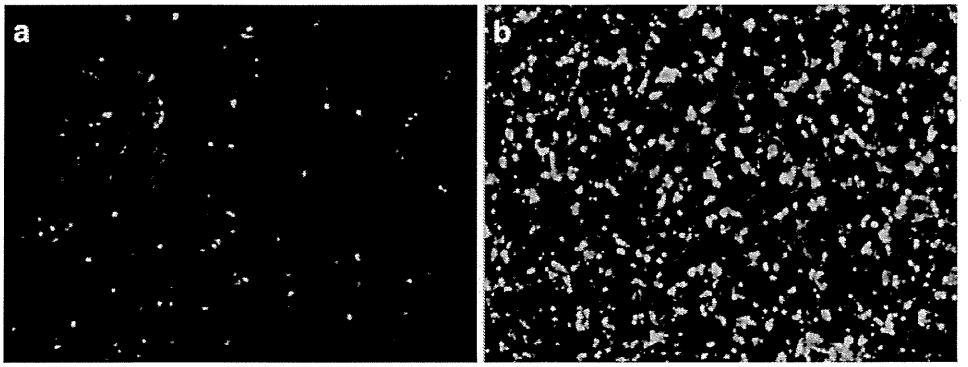

Fig. 3 Enhanced green fluorescent protein (EGFP) expression in CL6 cells using deacylated polyethylenimine (PEI max)-nanoparticle and magnetic field. Phase-contrast fluorescent micrograph of CL6 cells were transfected with pCAGGS-EGFP and PEI max as a control (**a**) and PEI max-nanoparticles (**b**). The numbers of EGFP-positive cells were further increased by PEI max-nanoparticles

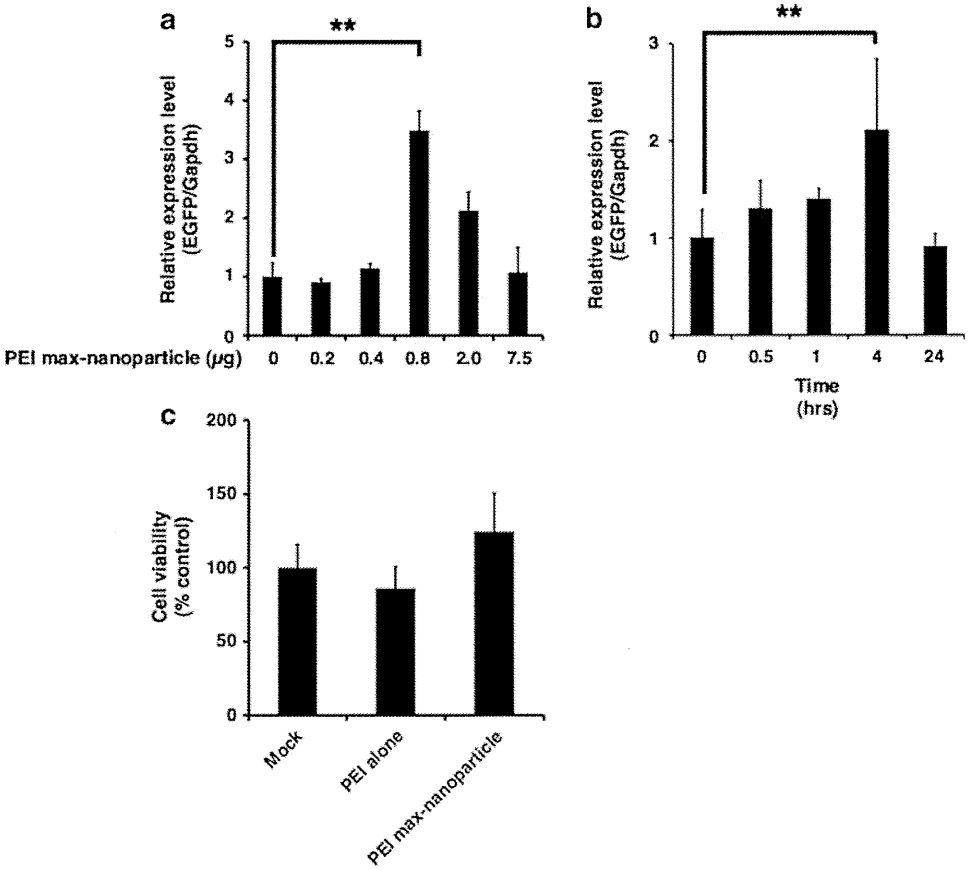

Fig. 4 Optimum condition for transfection of the deacylated polyethylenimine (PEI max)-nanoparticle. To optimize the transfection method, we examined PEI max-nanoparticles in terms of volume (**a**) and time (**b**) on the magnetic sheet. These results were evaluated by quantitative real-time reverse transcriptional polymerase chain reaction (RT-PCR). The expression level of the CL6 cells treated with PEI max alone is regarded as 1. The optimal conditions for transfection using PEI max-nanoparticles were when the CL6 cells were treated with 0.8 μg of PEI max-nanoparticles and 2.0 μg of pCAGGS-EGFP for 4 h on the magnetic sheet. The *double asterisks* indicate a significant difference ($P < 0.05$). Cytotoxicities of PEI max and PEI max-nanoparticles were evaluated by Alamar Blue assay (**c**). After 48 h of PEI max or PEI max-nanoparticle exposure, there were no significant differences in cell viability between CL6 cells treated with PEI max and those with PEI max-nanoparticles. *Mock* the CL6 cells treated without any treatment as a negative control. *PEI max alone* the CL6 cells treated with PEI max. *PEI max-nanoparticles* the CL6 cells treated with PEI max-nanoparticles (0.8 μg) for 4 h on the magnetic sheet. The relative absorbance of untreated CL6 cells is regarded as 100%

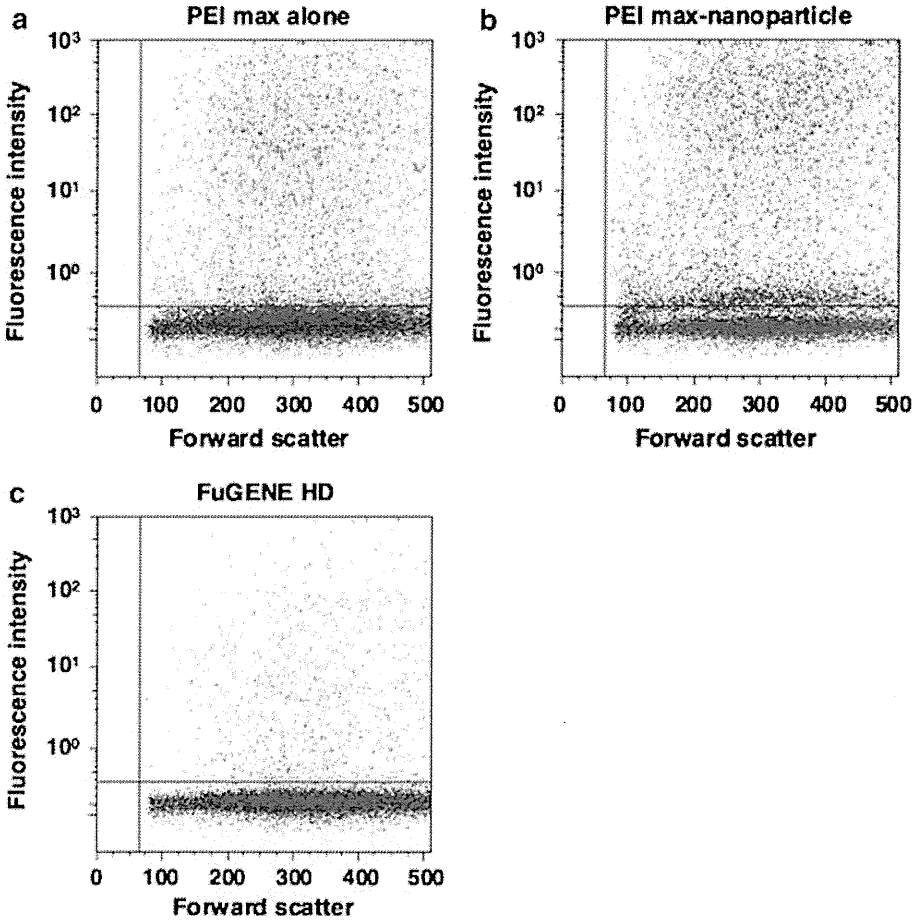

Fig. 5 Transfection efficiency of the deacylated polyethylenimine (PEI max)-nanoparticle. Comparison of scattering properties of the untreated CL6 cells (mock, *red dot*) and with PEI max alone (**a**, *blue dot*, 42.2 ± 8.5%), PEI max-nanoparticles (**b**, *blue dot*, 81.1 ± 4.0%), or FuGENE HD (**c**, *blue dot*, 13.9 ± 1.1%) by flow cytometry

Table 1 Comparison of transfection methods using the polyethylenimine and magnetic nanoparticles

Author	Year	Vector	Component	Cell	Transfection efficiency	Cell viability (% of control)	References
Kami	–	Plasmid	PEI max (MW 25k), MNP (γ-Fe2O3, 70 nm), MF (0.2 T)	P19CL6	80%[a]	100	This paper
Zhang	2010	Plasmid	Branched PEI (MW 25k), SPION (30 nm), MF (1.2 T)	NIH3T3	64%[a]	100	[14]
		siRNA	Branched PEI (MW 25k), SPION (30 nm), MF (1.2 T)	NIH3T3	77%[a]	100	
Kievit	2009	Plasmid	PEI (MW 25k), SPION (200 nm)	C6	90%[a]	10	[13]
		Plasmid	PEI (MW 25k), Chitosan, SPION (200 nm)	C6	45%[a]	100	
		Plasmid	PolyMag (commercial magnification reagent), MF (1.2 T)	C6	32%[a]	66	
Scherer	2002	Plasmid	PEI (MW 800k), SPION (200 nm), MF (1 T)	NIH3T3	5-fold[b]	–	[15]
		Adenovirus	PEI (MW 800k), SPION (200 nm), MF (1 T)	K562	100-fold[b]	–	
		Retrovirus	PEI (MW 800k), SPION (200 nm), MF (1 T)	NIH3T3	20%[a]	–	

Transfection efficiency indicates optimal transfection condition

PEI polyethylenimine, *PEI max* deacylated PEI, *MNP* magnetic nanoparticle, *SPION* superparamagnetic iron oxide nanoparticle, *MW* molecular weight, *MF* magnetic force, *T* tesla

[a] Flowcytometric analysis

[b] Luciferase activity assay

introducing plasmid into target cells with increased efficiency. Furthermore, a major advantage of this method is its tolerability among cells. Other methods might be limited either by possible cytotoxic effects of the lipidic transfection reagent (lipofection) or simply by the directly applied force on the cells (electroporation). In contrast, methods such as lipofection offer only a certain probability of hits between cargo and cells because of the three-dimensional motion of cells and transfection aggregates in a liquid suspension. Normally, transfection was inhibited

by serum using transfection reagent [25]. However, this method can also be performed in the presence of serum, which is a further benefit. Additionally, synergistic effects on transfection efficiency can arise from the possible combination of PEI max and nanoparticles. This technology might be an alternative to the currently used viral and nonviral vectors in gene therapy and gene transfer [26].

Our results suggest that PEI max-nanoparticles offer the ability to deliver various DNA formulations in addition to the traditional methods. Furthermore, gene transfer efficiency was not inhibited in the presence of serum in the cells. PEI max-nanoparticles may be a promising gene carrier with high transfection efficiency and low cytotoxicity.

Acknowledgments We express our sincere thanks to Koichiro Nishino (Department of Reproductive Biology, National Institute for Child Health and Development) for pCAGGS-EGFP. This study was supported by a Grant-in-Aid for the Global COE Program, Science for Future Molecular Systems from the Ministry of Education, Culture, Sports, Science and Technology, Japan (MEXT).

References

1. Kimura T, Iwai S, Moritan T, Nam K, Mutsuo S, Yoshizawa H, Okada M, Furuzono T, Fujisato T, Kishida A. Preparation of poly(vinyl alcohol)/DNA hydrogels via hydrogen bonds formed on ultra-high pressurization and controlled release of DNA from the hydrogels for gene delivery. J Artif Organs. 2007;10:104–8.
2. Moritake S, Taira S, Ichiyanagi Y, Morone N, Song SY, Hatanaka T, Yuasa S, Setou M. Functionalized nano-magnetic particles for an in vivo delivery system. J Nanosci Nanotechnol. 2007;7:937–44.
3. Tomitaka A, Koshi T, Hatsugai S, Yamada T, Takemura Y. Magnetic characterization of surface-coated magnetic nanoparticles for biomedical application. J Magn Magn Mater. 2010;323: 1396–1403.
4. Yokoyama M. Drug targeting with nano-sized carrier systems. J Artif Organs. 2005;8:77–84.
5. Lauterbur PC, et al. Image formation by induced local interactions. Examples employing nuclear magnetic resonance. Clin Orthop Relat Res. 1973;1989:3–6.
6. Nakamura H, Ito N, Kotake F, Mizokami Y, Matsuoka T. Tumor-detecting capacity and clinical usefulness of SPIO-MRI in patients with hepatocellular carcinoma. J Gastroenterol. 2000;35: 849–55.
7. Karlsson HL, Cronholm P, Gustafsson J, Moller L. Copper oxide nanoparticles are highly toxic: a comparison between metal oxide nanoparticles and carbon nanotubes. Chem Res Toxicol. 2008; 21:1726–32.
8. Karlsson HL, Gustafsson J, Cronholm P, Moller L. Size-dependent toxicity of metal oxide particles–a comparison between nano- and micrometer size. Toxicol Lett. 2009;188:112–8.
9. Boussif O, Lezoualc'h F, Zanta MA, Mergny MD, Scherman D, Demeneix B, Behr JP. A versatile vector for gene and oligonucleotide transfer into cells in culture and in vivo: polyethylenimine. Proc Natl Acad Sci USA. 1995;92:7297–301.
10. Wang J, Gao L. Adsorption of polyethylenimine on nanosized zirconia particles in aqueous suspensions. J Colloid Interface Sci. 1999;216:436–9.
11. Vancha AR, Govindaraju S, Parsa KV, Jasti M, Gonzalez-Garcia M, Ballestero RP. Use of polyethyleneimine polymer in cell culture as attachment factor and lipofection enhancer. BMC Biotechnol. 2004;4:23.
12. Thomas M, Lu JJ, Ge Q, Zhang C, Chen J, Klibanov AM. Full deacylation of polyethylenimine dramatically boosts its gene delivery efficiency and specificity to mouse lung. Proc Natl Acad Sci USA. 2005;102:5679–84.
13. Kievit FM, Veiseh O, Bhattarai N, Fang C, Gunn JW, Lee D, Ellenbogen RG, Olson JM, Zhang M. PEI-PEG-chitosan copolymer coated iron oxide nanoparticles for safe gene delivery: synthesis, complexation, and transfection. Adv Funct Mater. 2009;19:2244–51.
14. Zhang H, Lee MY, Hogg MG, Dordick JS, Sharfstein ST. Gene delivery in three-dimensional cell cultures by superparamagnetic nanoparticles. ACS Nano. 2010;4:4733–43.
15. Scherer F, Anton M, Schillinger U, Henke J, Bergemann C, Kruger A, Gansbacher B, Plank C. Magnetofection: enhancing and targeting gene delivery by magnetic force in vitro and in vivo. Gene Ther. 2002;9:102–9.
16. Bertram J. MATra—magnet assisted transfection: combining nanotechnology and magnetic forces to improve intracellular delivery of nucleic acids. Curr Pharm Biotechnol. 2006;7: 277–85.
17. Arsianti M, Lim M, Marquis CP, Amal R. Polyethylenimine based magnetic iron-oxide vector: the effect of vector component assembly on cellular entry mechanism, intracellular localization, and cellular viability. Biomacromolecules. 2010;11:2521–31.
18. Georgieva JV, Kalicharan D, Couraud PO, Romero IA, Weksler B, Hoekstra D, Zuhorn IS. Surface characteristics of nanoparticles determine their intracellular fate in and processing by human blood-brain barrier endothelial cells in vitro. Mol Ther. 2011; 19:318–25.
19. Longmire M, Choyke PL, Kobayashi H. Clearance properties of nano-sized particles and molecules as imaging agents: considerations and caveats. Nanomedicine (Lond). 2008;3:703–17.
20. Niwa H, Yamamura K, Miyazaki J. Efficient selection for high-expression transfectants with a novel eukaryotic vector. Gene. 1991;108:193–9.
21. Nakayama GR, Caton MC, Nova MP, Parandoosh Z. Assessment of the Alamar blue assay for cellular growth and viability in vitro. J Immunol Methods. 1997;204:205–8.
22. Namgung R, Singha K, Yu MK, Jon S, Kim YS, Ahn Y, Park IK, Kim WJ. Hybrid superparamagnetic iron oxide nanoparticle-branched polyethylenimine magnetoplexes for gene transfection of vascular endothelial cells. Biomaterials. 2010;31:4204–13.
23. Song HP, Yang JY, Lo SL, Wang Y, Fan WM, Tang XS, Xue JM, Wang S. Gene transfer using self-assembled ternary complexes of cationic magnetic nanoparticles, plasmid DNA and cell-penetrating Tat peptide. Biomaterials. 2010;31:769–78.
24. Coonrod A, Li FQ, Horwitz M. On the mechanism of DNA transfection: efficient gene transfer without viruses. Gene Ther. 1997;4:1313–21.
25. Purow BW, Sundaresan TK, Burdick MJ, Kefas BA, Comeau LD, Hawkinson MP, Su Q, Kotliarov Y, Lee J, Zhang W, Fine HA. Notch-1 regulates transcription of the epidermal growth factor receptor through p53. Carcinogenesis. 2008;29:918–25.
26. Davis ME. Non-viral gene delivery systems. Curr Opin Biotechnol. 2002;13:128–31.

J Orthop Sci (2011) 16:670–672
DOI 10.1007/s00776-011-0119-2

RAPID SHORT COMMUNICATION

Gene expression profiling of mouse growth plate cartilage by laser microdissection and microarray analysis

Honoka Isshiki · Kazuki Sato · Keisuke Horiuchi · Shuichi Tsutsumi · Makoto Kano · Hiroyasu Ikegami · Hitoshi Abe · Akihiro Umezawa · Hiroyuki Aburatani · Yoshiaki Toyama

Received: 4 April 2011 / Accepted: 9 June 2011 / Published online: 1 July 2011

Introduction

Longitudinal bone growth results from a complex sequence of events involving differentiation of resting chondroblasts into proliferative, pre-hypertrophic, and hypertrophic chondrocytes. The growth plate (epiphyseal plate), which is primarily responsible for longitudinal growth, can be divided into four distinct zones: the resting zone (RZ), proliferating zone (PZ), maturing zone (MZ), and hypertrophic zone (HZ), on the basis of the morphology of the developing chondroblasts and the structure of the cartilage matrix. In the past two decades substantial progress has been made in understanding the mechanisms underlying chondroblast differentiation and skeletal development [1–3]. However, comprehensive analysis of gene expression patterns in the growth plate has been technically challenging.

In this study, we performed a gene expression profile analysis of each zone of the growth plate from 9-day-old mice, using microdissection and microarray analysis, and determined the expression profiles of 1,995 genes in the murine growth plate. Furthermore, we have created a publicly available and searchable on-line database [murine growth plate database (MGPDB)] containing the gene expression data from this study (http://157.82.78.238/mgpdb/main_search.jsp). We believe this will serve as a useful tool for researchers in the field of skeletal development.

H. Isshiki · K. Sato (✉) · K. Horiuchi · H. Ikegami · Y. Toyama
Department of Orthopedic Surgery, School of Medicine, Keio University, 35 Shinanomachi, Shinjuku-ku, Tokyo 160-8582, Japan
e-mail: kazuki@sc.itc.keio.ac.jp

S. Tsutsumi · H. Aburatani
Genome Science Division, Research Center for Advanced Science and Technology, The University of Tokyo, Tokyo, Japan

M. Kano
Intelligent Cooperative System, Department of Information Systems, Research Center for Advanced Science and Technology, The University of Tokyo, Tokyo, Japan

H. Abe
Department of Pathology, School of Medicine, Keio University, Tokyo, Japan

A. Umezawa
Department of Reproductive Biology, National Research Institute for Child Health and Development, Tokyo, Japan

Results and discussion

Two 9-day-old male ICR mice were used for the analysis. The tibiae were harvested, embedded in OCT, and immediately frozen in liquid nitrogen. Forty cryosections 10 μm thick were prepared, and the tissues from each growth plate zone were identified and collected using a laser microdissection microscope (Fig. 1a). All animal experiments were approved by the Institutional Animal Care and Use Committee of the School of Medicine, Keio University. The samples from each individual mouse (#1 and #2) were analyzed separately. The gene expression profiles in the collected samples were analyzed using the GeneChip Mouse Genome 430 2.0 Array and Affymetrix Microarray Suite v5.0 (Affymetrix). Approximately 14,500 transcripts (out of 45,101 probes on the chip) whose signal intensity was above the detection level, were further filtered to eliminate those transcripts expressed at a very low level, or those hybridized to a non-functional probe. Finally, 2,427

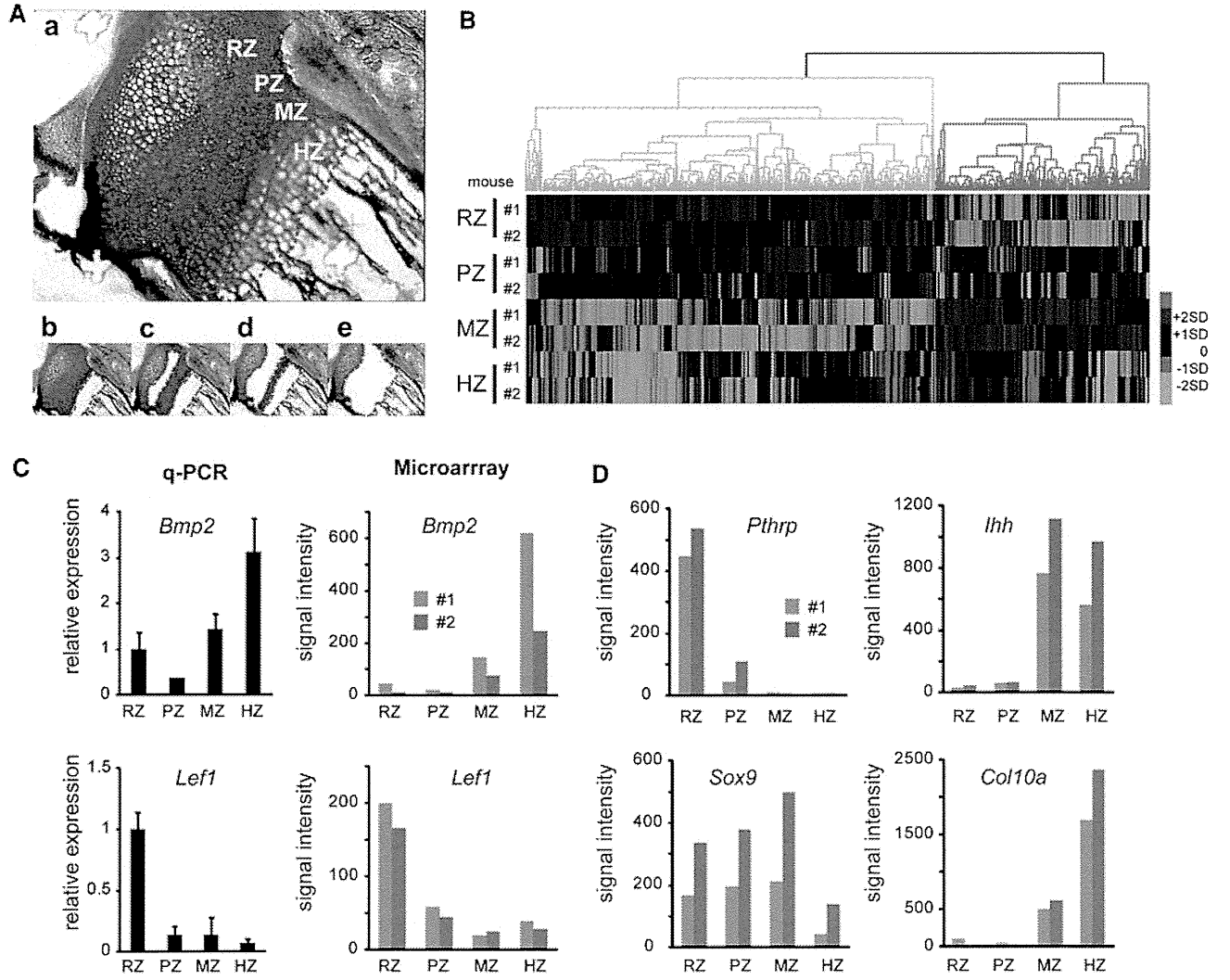

Fig. 1 **a** Representative photomicrographs for the laser microdissection procedure. *a* Sagittal cryosection of the tibia stained with Giemsa. Areas circumscribed by *broken lines* represent each zone of the growth plate. Tissue from these sections was sequentially harvested from the HZ (*b*), RZ (*c*), PZ (*d*), and MZ (*e*). **b** Hierarchical clustering dendrogram and heat map showing 1,955 genes expressed in the growth plate. Gene expression profiles of two individual mice (#1 and #2) are presented. Relatively tight clustering was seen in the genes expressed in the RZ and PZ (*yellow*), and in the MZ and HZ (*blue*). **c** Expression patterns of the transcripts for *Bmp2* and *Lef1* evaluated by qPCR and microarray analysis. Gene expression levels of the two individual mice (#1 and #2) deduced from the microarray analysis are presented. **d** Expression profiles of *Pthrp*, *Ihh*, *type 10 collagen* (*Col10a*), and *Sox9* in the two individual mice (#1 and #2) deduced from the microarray analysis

transcripts, corresponding to 1,995 different genes, were identified. Detailed description of the procedures, including RNA extraction, cRNA probe labeling, gene chip hybridization, and data analysis, will be provided on request.

To obtain an overview of the gene expression profiles, we first performed hierarchical clustering analysis of the transcripts expressed in each zone of the growth plates from two individual mice. As shown in Fig. 1b, it was clear from this analysis that the gene expression profiles of each growth plate zone were highly reproducible between the individual mice. Interestingly, we found that the dendrogram divided into two main branches: the gene clusters expressed in the early stage of differentiation of chondroblasts (RZ and PZ), and those expressed in the later stage (MZ and HZ) (Fig. 1b), indicating that chondroblasts undergo drastic changes in their gene expression profile during their transition from PZ to MZ.

To confirm that the RNA amplification and data processing did not skew the actual expression patterns of the transcripts in vivo, we compared the expression levels of several genes deduced from the microarray analysis with those evaluated by quantitative PCR (qPCR). As illustrated by the examples shown in Fig. 1c, *Bmp2* (which is predominantly expressed in the HZ) and *Lef1* (a transcriptional mediator of Wnt/β-catenin signaling), we found a significant correlation in the expression patterns of all the

genes we examined, suggesting that the gene expression levels deduced from the microarray analysis in this study were comparable with those measured by qPCR.

We next examined the expression patterns of several genes whose functions and expression patterns in the growth plate have been well characterized, to evaluate whether our data could reproduce previous findings. For example, the feedback loop between *Pthrp* and *Ihh* in the growth plate plays an essential role in longitudinal skeletal growth [2], and the expression of these genes is known to be mutually exclusive in vivo; the transcripts for *Pthrp* are found in the RZ, and those for *Ihh* in the HZ. As shown in Fig. 1d, our data sets clearly reproduced this observation. Furthermore, the expression profiles of *type 10 collagen* (which is specifically expressed in the HZ) and *Sox9* (which is induced in the RZ, PZ, and MZ, but not in the HZ), were also consistent with past studies [3]. Taken together, these findings indicate that our sampling of tissue from each growth plate zone was accurate, and that the expression profiles deduced from microarray analysis reflected the actual expression patterns of a given gene in vivo, with high reproducibility.

Because of the difficulty of obtaining tissue from each of the specific zones of the murine growth plate in terms of both quantity and quality, it has been difficult to perform comprehensive analysis of the expression profiles of genes in the growth plate. Here, using a combination of laser microdissection and microarray analysis, we have successfully established a data set that contains the expression profiles of 1,995 different genes expressed in the growth plate. Although similar studies have been reported [4–6], our study is unique in three respects:

1. the data were obtained by use of a mouse genome expression array containing 45,100 probes and approximately 34,000 genes, which enabled the most comprehensive analysis of genome-wide expression currently available;
2. by using a laser microdissection microscope, cartilage tissue was collected from the four distinct zones in the growth plate with high accuracy, enabling precise spatial analysis of the gene expression patterns; and
3. the data set was made publicly available for investigators via an on-line database.

The mechanisms governing the differentiation of chondroblasts in the growth plate are very complex, and many of the molecular mechanisms behind skeletal development remain to be elucidated. We believe that the gene expression data established in this study will facilitate further investigation in this field.

Conflict of interest The authors declare no conflict of interest.

References

1. Karsenty G, Wagner EF. Reaching a genetic and molecular understanding of skeletal development. Dev Cell. 2002;2:389–406.
2. Kronenberg HM. Developmental regulation of the growth plate. Nature. 2003;423:332–6.
3. Adams SL, Cohen AJ, Lassova L. Integration of signaling pathways regulating chondrocyte differentiation during endochondral bone formation. J Cell Physiol. 2007;213:635–41.
4. Belluoccio D, Bernardo BC, Rowley L, Bateman JF. A microarray approach for comparative expression profiling of the discrete maturation zones of mouse growth plate cartilage. Biochim Biophys Acta. 2008;1779:330–40.
5. Wang Y, Middleton F, Horton JA, Reichel L, Farnum CE, Damron TA. Microarray analysis of proliferative and hypertrophic growth plate zones identifies differentiation markers and signal pathways. Bone. 2004;35:1273–93.
6. Benoyahu D, Akavia UD, Socher R, Shur I. Gene expression in skeletal tissues: application of laser capture microdissection. J Microsc. 2005;220:1–8.

STEM CELLS®

STEM CELL TECHNOLOGY: EPIGENETICS, GENOMICS, PROTEOMICS, AND METABONOMICS

Treatment of Human Mesenchymal Stem Cells with Angiotensin Receptor Blocker Improved Efficiency of Cardiomyogenic Transdifferentiation and Improved Cardiac Function via Angiogenesis

YOHEI NUMASAWA,[a] TAKEHIRO KIMURA,[a] SHUNICHIRO MIYOSHI,[a] NOBUHIRO NISHIYAMA,[a] NAOKO HIDA,[a] HIROKO TSUJI,[a] HIKARU TSURUTA,[a] KAORU SEGAWA,[b] SATOSHI OGAWA,[a] AKIHIRO UMEZAWA[c]

[a]Department of Cardiology and [b]Department of Microbiology and Immunology, Keio University School of Medicine, Tokyo, Japan, [c]Department of Reproductive Biology and Pathology, National Research Institute for Child Health and Development, Tokyo, Japan

Key Words. Angiotensin • Bone marrow stromal cells • Transdifferentiation • Stem cell transplantation

ABSTRACT

To improve the modest efficacy of mesenchymal stem cell (MSC) transplantation, the treatment of human MSCs with angiotensin receptor blockers (ARBs) was investigated. MSCs were cultured with or without the medium containing 3 μmol/l of ARBs before cardiomyogenic induction. After cardiomyogenic induction in vitro, cardiomyogenic transdifferentiation efficiency (CTE) was calculated by immunocytochemistry using anticardiac troponin-I antibody. In the nude rat chronic myocardial infarction model, we injected MSCs pretreated with candesartan (A-BM; $n = 18$) or injected MSCs without pretreatment of candesartan (BM; $n = 25$), each having survived for 2 weeks. The left ventricular function, as measured by echocardiogram, was compared with cardiomyogenic transdifferentiation in vivo, as determined by immunohistochemistry. Pretreatment with ARBs significantly increased the CTE in vitro (10.1 ± 0.8 $n = 12$ vs. $4.6 \pm 0.3\%$ $n = 25$, $p < .05$). Transplantation of candesartan-pretreated MSCs significantly improved the change in left ventricular ejection fraction (BM; -7.2 ± 2.0 vs. A-BM; $3.3 \pm 2.3\%$). Immunohistochemistry revealed significant improvement of cardiomyogenic transdifferentiation in A-BM in vivo (BM; 0 ± 0 vs. A-BM; $0.014 \pm 0.006\%$). Transplantation of ARB-pretreated MSCs significantly improved cardiac function and can be a promising cardiac stem cell source from which to expect cardiomyogenesis. STEM CELLS *2011;29:1405–1414*

Disclosure of potential conflicts of interest is found at the end of this article.

INTRODUCTION

Regeneration therapies have attracted a great deal of medical attention. Various cellular resources such as embryonic stem cells [1], mesenchymal stem cells (MSCs) [2], mononuclear cells [3, 4], and endothelial progenitor cells (EPCs) [5] have been candidates for the regeneration therapies. The majority of cells derived from bone marrow (BM) consist of blood cells in various stages of differentiation; however, BM also contains, hematopoietic stem cells, EPCs, and MSCs. MSCs have characteristics of replication competence and multipotency [2, 6–8], as reported in numerous studies of MSCs.

Mesenchymal cells are classified as somatic stem cells and exist in BM stroma, dermis, skeletal muscle, uterine endometrial gland [9], umbilical cord blood [7, 10], placenta [11], amniotic membrane [6], etc. They are known to be capable of transdifferentiating into bone, cartilage, skeletal muscles, fats, ligaments, vascular endothelium, smooth muscle, and cardiomyocytes. Among the various mesenchymal cell sources, BM-derived MSCs (BM-MSCs) can be used in an autologous manner; therefore, there are no immunological problems in transplantations. However, in terms of cardiomyogenic transdifferentiation, the efficiency of human BM-MSCs is extremely low [8] in vitro, and efficiency of human BM-MSC transplantation is modest in in vivo [12, 13] and in clinical trials [14, 15]. The limited effect in clinical trials may be due to low angiogenic and paracrine effect of human BM-MSCs, low cardioprotective effect on host myocardium, and partially due to low cardiomyogenic transdifferentiation efficiency (CTE) [8]. We have previously shown that human mesenchymal cells derived from younger populations, that is,

Author contributions: Y.N., T.K., N.N., H. Tsuji, H. Tsuruta, and K.S.: conception and design, collection and assembly of data, final approval of manuscript; S.M.: conception and design, administrative support, collection and assembly of data, data analysis and interpretation, manuscript writing, final approval of manuscript; N.H.: conception and design, collection and assembly of data; S.O.: financial support, administrative support, final approval of manuscript; A.U.: financial support, administrative support, final approval of manuscript. Y.N. and T.K. contributed equally to this article.

Correspondence: Shunichiro Miyoshi, M.D., Ph.D., Keio University School of Medicine, 35-Shinanomachi, Shinjuku-ku, Tokyo 160-8582, Japan. Telephone: 81-3-3353-1211, ext. 61421; Fax: 81-3-5363-3875; e-mail: smiyoshi@cpnet.med.keio.ac.jp Received March 8, 2011; accepted for publication June 30, 2011; first published online in STEM CELLS *EXPRESS* July 13, 2011.
1066-5099/2009/$30.00/0 doi: 10.1002/stem.691

endometrial gland [9], umbilical cord blood [10], placenta [11], and amniotic membrane [6] have a high CTE and a beneficial effect on cardiac function. Therefore, we hypothesized that mesenchymal cells obtained from younger populations might have a better effect on regeneration therapies. As angiotensin receptor blocker (ARB) was known to have the potential to play a role in the anti-aging effect, we postulated that ARB might improve the efficacy of BM-MSCs on cardiac stem cell therapy.

Stimulation of angiotensin receptors is known to be related to adipogenic transdifferentiation of human BM-MSCs [16]. In the brain ischemic reperfusion model, BM-MSC transplantation significantly reduced the brain infarction area via improvement of brain blood flow and reduction of oxidative stress [17]. The effect of BM-MSC transplantation was abolished by knocking out the angiotensin-II (AT) receptor type-II (AT2R). On the other hand, this effect was restored by pretreatment with ARB for BM-MSCs in the culture. These facts suggest that ARB and stimulation of AT receptor may play a significant role in causing the angiogenesic effect of BM-MSC transplantation. Therefore, in this study, we investigated the effect of ARB on CTE of human BM-MSCs in vitro and in vivo, and efficacy of BM-MSC transplantation on cardiac function in the myocardial infarction (MI) model in vivo.

Materials and Methods

BM-Derived MSCs

Yub623 (RIKEN Cell bank, Cell No. HMS0017, Tokyo, Japan) cells were used as BM-MSCs in this study. Yub623 is a fibroblast-like shaped human MSC (hMSC) derived from neonatal human BM from a finger of patients with polydactyly. Cells were cultured in high-glucose supplemented Dulbecco's modified Eagle's medium containing 10% human serum.

Cardiomyogenic Induction and Chemical Agents

The method of cardiomyogenic induction in vitro was described previously (Supporting Information Material and Method-1) [6, 8–11]. In short, enhanced green fluorescent protein (EGFP) labeled BM-MSCs were cocultured with murine cardiomyocytes. In this system, the incidence of cell fusion was approximately 0.3% and the evidence of cell fusion-independent cardiomyogenesis was extensively shown in the previous studies [6, 8–11, 18, 19]. BM-MSCs were preincubated with chemical agent-containing medium for 2 weeks before coculture and/or cultured with chemical agent-containing medium after coculture. In this study, we used 3 μmol/l of telmisartan (tel), candesartan (cnd), losartan (los), olmesartan (olm), and valsartan (val) as an AT receptor blocker (ARB), 3 μmol/l of PD123319 (pd) as a specific AT type-I blocker; enalaprilat (ena) and captopril (cap) as an angiotensin converting enzyme (ACE) inhibitor; 3 μmol/l of aliskiren (ali) as a direct rennin inhibitor; 1 μmol/l of AT; and 10 μmol/l of GW9662 (gw) as a peroxisome proliferators-activated receptor-γ (PPAR-γ) blocker. Evaluation of efficiency of cardiomyogenic transdifferentiation was described previously [6, 10, 11]. In short, cocultivated BM-MSCs were enzymatically isolated, a smear sample was made, and then immunocytochemistry using mouse monoclonal antibody against anticardiac troponin-I (Trop-I, #4T21 Hytest, Euro, Finland) antibody was performed (described later). Isolated cells (spherical shape), in which Trop-I colocalized with EGFP at the cytoplasm were considered as Trop-I/EGFP double positive cells. The CTE was defined as the incidence of Trop-I/EGFP double positive cells in EGFP-positive BM-MSCs. The incidence of cell fusion was not affected by ARB treatment (0.30% to 0.39%) in this study.

Immunocytochemistry and Immunohistochemistry

A laser confocal microscope (FV1000, Olympus, Tokyo, Japan) was used. As described previously [6, 8–11, 18, 19], samples were stained with Trop-I with mouse monoclonal antibody (sigma) and rabbit polyclonal anti-connexin 43 antibody (sigma) diluted 1:300 overnight at 4°C, then stained with TRITC-conjugated anti-mouse IgG antibody (Sigma) and Cy5-conjugated anti-rabbit IgG antibody (Chemicon) diluted 1:100, containing 4′-6-diamidino-2-phenylindole (Wako) at 1:300 for 30 minutes at 25–28°C.

Enzyme-Linked Immunosorbent Assay

Angiogenic humoral factors (angiogenin, angiotensin-2, epidermal growth factor [EGF], basic fibroblast growth factor, heparin-binding EGF-like growth factor, hepatocyte growth factor, phosphatidylinositol-glycan biosynthesis class F protein, and vascular endothelial growth factor) in culture medium supernatant (cultured with 10% serum-containing medium for 7 days) were measured by enzyme-linked immunosorbent assay [19]. The assay was performed with Quantibody Human Angiogenesis Array I kit (RayBiotec, Inc. GA) and was conducted according to manufacturer recommended protocol.

Gene Chip Analysis

Human genome-wide gene expression was examined with the Human Genome U133A Probe array (Affymetrix), which contains the oligonucleotide probe set for approximately 23,000 full-length genes and expressed sequence tags as described previously [11, 20].

Transplantation of ARB-Pretreated BM-MSCs in MI Model In Vivo

MI was induced in the open chests of anesthetized female F344 nude rats (Clea Japan, Inc., 6 weeks of age) as described previously [6, 9, 19]. Two weeks after MI, 1–2 $\times$ 10^6 of EGFP-labeled BM-MSCs were injected into the myocardium at the border zone of the MI. Two weeks after the first operation, rats with MI were randomized in a blind study of the following groups: the sham operated group (Sham), the (CNT), the CNT with plain BM-MSC transplanted group (BM), and the MI+candesartan-pretreated BM-MSC transplanted group (A-BM). After cellular transplantation, TCV-116 (stable form of candesartan; 0.5 mg/kg/day) was orally administered in some of the experiments (+A). Randomization occurred immediately before echocardiogram. Immediately before cell transplantation, two-dimensional and M-mode echocardiographic (8.5 MHz linear transducer; EnVisor C, Phillips Medical System, Andover, MA) images were obtained to assess left ventricular (LV) end-diastolic dimension and LV end-systolic dimension (LVESD) at the mid-papillary muscle level by a single blinded observer. Two weeks after the transplantation, a similar echocardiogram was performed again. LV percentage fractional shortening, thickness of anterior wall (AW), and thickness of posterior wall were calculated from five to six traces and averaged. LV pressure, brain natriuretic peptide (BNP), body weight, and heart weight (wet) were measured as described previously. Tissue samples were obtained by slicing along the short axis of the left ventricle, for every 1 mm of depth. After masson trichrom staining, the area of fibrosis was digitized from each slice, and then the percentage fibrosis volume in the LV myocardium was calculated as described previously [6, 19]. Immunohistochemical analysis was performed to observe CTE in vivo as described previously (Supporting Information Material and Method-2). Immunohistochemical analysis was performed using anti-rat CD34 antibody (1:200 R&D Systems; AF4117) to evaluate vascular density. Then, biotinylated goat immunoglobulins (Dako; E0466) were used as a second antibody, next, strept avidin biotin complex (ABC) complex/horseradish peroxidase (HRP) (Dako; K0377), and, finally, 3,3′-Diaminobenzidine substrate (Wako; K3183500) were used. The images were digitized and the percentage brown pixel area of the capillary vessels was counted in the peri-infarct normal zone (NZ) and the center of the MI

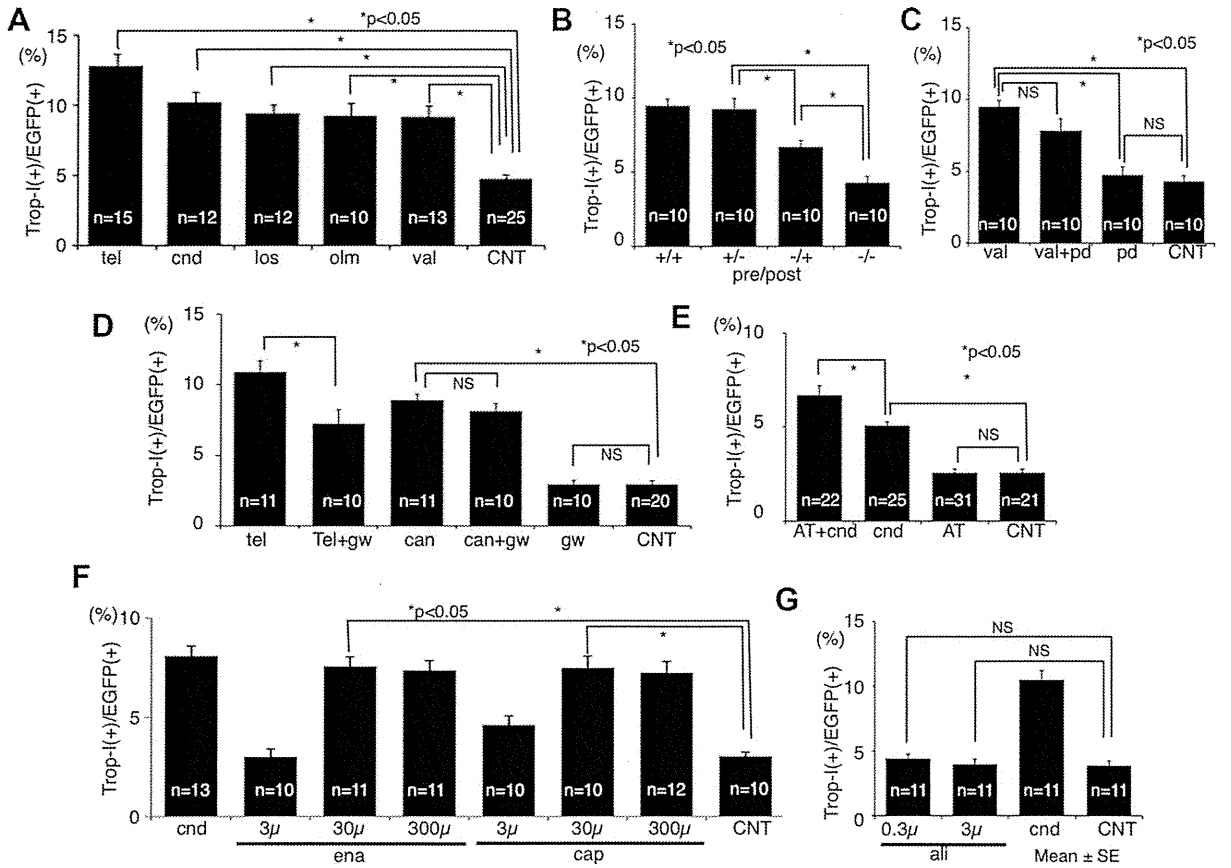

Figure 1. Improvement of cardiomyogenic transdifferentiation efficiency (CTE) of bone marrow-derived mesenchymal stem cells (BM-MSC) by blockade of renin-angiotensin system in vitro. The calculated rate of cardiac troponin-I positive cells in enhanced green fluorescent protein-positive cells are averaged and shown as CTE. **(A):** The effect of pretreatment with telmisartan (tel), candesartan (cnd), losartan (los), olmesartan (olm), and valsartan (val) on CTE of human BM-MSCs are shown. CNT denoted CTE of control MSCs. These ARBs increase CTE significantly. **(B):** Condition of pretreatment of val (before slash) and val treatment after induction (after slash) are shown in the bottom. Pretreatment of val significantly increased CTE and was essential for val-induced CTE increase. Val treatment after induction moderately increased CTE. **(C):** The effect of combination of val as a specific angiotensin-II (AT) receptor type-I (AT1R) blocker and PD123319 (pd) as a specific AT2R blocker to CTE is shown. The pd did not affect CTE. **(D):** The effect of GW9662 (gw) as a specific peroxisome proliferators-activated receptor-γ (PPAR-γ) blocker on tel-induced CTE increase and cnd-induced CTE increase are shown. The blockade of PPAR-γ partially blocked the tel-induced CTE increase and did not affect cnd-induced CTE increase. **(E):** The effect of additional application AT in the presence or in the absence of cnd is shown. AT alone did not affect CTE; however, AT significantly increased CTE in the presence of cnd. **(F):** Dose-response effect of pretreatment with enalaprilat (ena) and captoril (cap) as angiotensin converting enzyme inhibitors (ACEI). ACEI significantly improves CTE in a dose-dependent manner. **(G):** The effect of aliskiren (ali) as a renin inhibitor on CTE is shown. Ali did not affect CTE. *p<0.05. Abbreviations: ali, aliskiren; AT, angiotensin-II; cap, captoril; cnd, candesartan; CNT, control; EGFP, enhanced green fluorescent protein; ena, enalaprilat; gw, GW9662; los, losartan; olm, olmesartan; pd, PD123319; Tel, telmisartan; Trop-I, troponin-I; val, valsartan.

zone (MI) using a light microscope at 10× magnification. The areas in five high-power fields were calculated and averaged.

Statistical Analysis

All data are shown as mean value ± SE. The difference between mean values was determined with one-way analysis of variance (ANOVA) test or one-way repeated measures ANOVA test and Bonferroni post hoc test. Statistical significance was set at $p < .05$.

Results

Pretreatment with ARB Increased Efficiency of Cardiomyogenic Transdifferentiation Via AT2R

Administration of 3 μmol/l of popular ARBs (tel, can, los, olm, and val) did not cause any significant change in morphology of BM-MSCs (Supporting Information Fig. 1A, 1B), while improved CTE in vitro was observed (Fig. 1A and Supporting Information Fig. 1C–1P). In our pilot study, we tested dose-response effect of ARBs and confirmed that this effect was saturated at the concentration of 3 μmol/l (CTE at control, 0.03, 0.3, 3, and 30 μmol/l of cnd were 3.0 ± 0.3, 3.5 ± 0.2, 4.8 ± 0.3, 8.9 ± 0.4, and 8.1 ± 0.5%, respectively). Therefore, in this study, we selected 3 μmol/l as a default concentration of ARBs. To clarify the target of the ARBs, val was administrated only before the coculture or only after the coculture (Fig. 1B). Administration of val after the start of coculture (±) caused modest improvement of CTE; on the other hand, administration of val before the start of coculture (±) significantly increased CTE, suggesting that val modified the character of the BM-MSCs so as to be able to cause higher CTE. To determine whether the effect of the ARBs was mediated by AT receptor type-I (AT1R) or AT2R, we used val as AT1R specific blocker and pd as AT2R specific blocker (Fig. 1C). Administration of pd did not affect CTE, while val increased CTE significantly. Furthermore, CTE with both val and pd administered did not show an additional increase

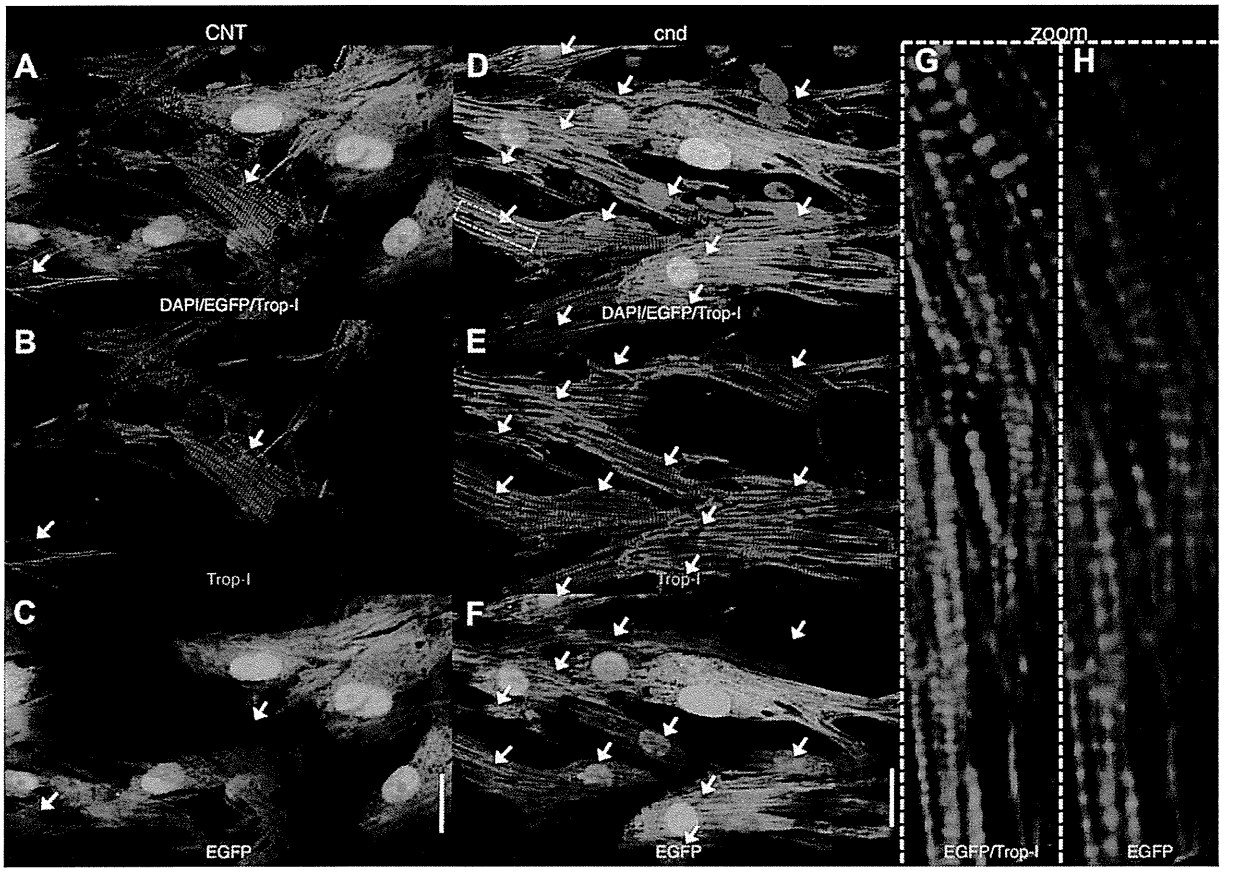

Figure 2. Confocal laser microscopic images of the immunocytochemical analysis of transdifferentiated cardiomyocytes. Confocal microscopic images of immunocytochemistry after cardiomyogenic induction using anti-cardiac troponin-I (red: Trop-I) revealed significant augmentation of enhanced green fluorescent protein (EGFP) (green)/Trop-I double positive cardiomyocytes (white arrow) by candesartan (cnd) (**D–F**) pretreatment, while EGFP/Trop-I double positive cells were rare in CNT (**A–C**). Area within the dotted yellow box is expanded and shown in (**G, H**). Clear striation staining pattern of Trop-I was observed in every EGFP-positive cell. The striating pattern of EGFP and Trop-I appeared in alternation, suggesting that the Trop-I was expressed in the EGFP-positive cells. Scale bar = 20 μm. Abbreviations: cnd, candesartan; CNT, control; DAPI, 4′-6-diamidino-2-phenylindole; EGFP, enhanced green fluorescent protein; Trop-I, troponin-I.

(rather, tended to show a statistically nonsignificant decrease). These data suggest that blockade of AT1R plays a pivotal role in ARB-dependent CTE increase. We have previously reported that PPAR-γ activator has an ability to increase CTE of BM-MSCs [19], and some of the ARBs, that is, tel, have a potential to activate the PPAR-γ. To clarify that the mechanism of ARB-induced CTE increase was mediated via PPAR-γ activation effect, we used gw as a specific blocker for PPAR-γ (Fig. 1D). The gw partially blocked tel-induced CTE increase; on the other hand, it did not block cnd-induced CTE increase. These data suggest that the effect of cnd on CTE was independent from PPAR-γ activation. In our previous study, the effect of pio was completely blocked by gw [19]; therefore, the gw-insensitive tel-induced CTE increase was caused by a PPAR-γ-independent mechanism. On the other hand, administration of AT did not affect CTE in the absence of ARB, while administration of AT significantly increased CTE in the presence of ARB (Fig. 1E). These data suggest both blockade of AT1R and stimulation of AT2R increase CTE. The increase in CTE was also observed by administration of ACE inhibitors ena or cap (Fig. 1F), suggesting the source of AT in this system is autocrine of angiotensin-I from BM-MSCs and local ACE activity. Furthermore, the effect was not blocked by the specific renin blocker, ali (Fig. 1G); therefore, angiotensinogen does not play a role as an AT source in this system, but a local angiotensin-generating system may play a role in this phenomenon.

The Effect of ARB-Treated BM-MSC Transplantation on Cardiac Function In Vivo

The BM-MSCs were transplanted into the hearts of nude rats with chronic MI, in vivo, and the effect on cardiac function was examined. Representative M-mode echocardiographic images at 2 weeks after transplantation are shown (Fig. 2A). In the CNT group, akinesis and thinning of AW are observed. There were no marked changes in the BM group, while in A-BM group, the motion of AW markedly improved. The same trend was also observed in the ARB orally administered group (+A group). The changes in echocardiographic parameters between the immediately before the transplantation group (post MI 2 weeks) and the 2 weeks after transplantation group (post MI 4 weeks) are compared (Fig. 3). Changes in LV ejection fraction (ΔLVEF) were decreased as a function of time, even 2 weeks after the MI, which may be due to LV remodeling. The transplantation of plain BM-MSCs (BM) did not have an effect on ΔLVEF; on the other hand, candesartan-pretreated BM-MSCs (A-BM) significantly improved ΔLVEF. The degree of improvement was marked when candesartan was orally administered (A-BM-A). Change in end-diastolic diameter of LV (ΔLVEDD) did not differ among the

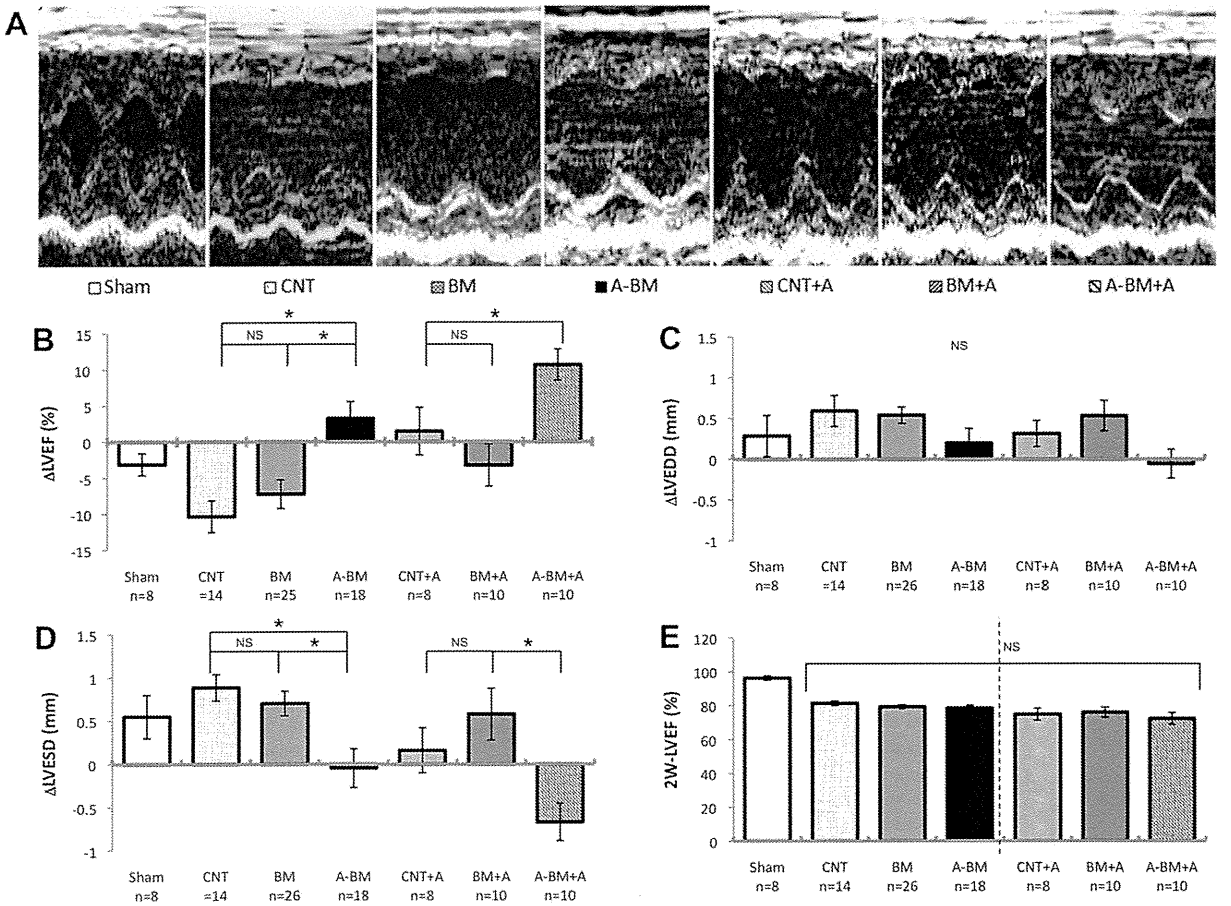

Figure 3. Effect of candesartan-pretreated bone marrow-derived mesenchymal stem cell (BM-MSC) transplantation and/or oral administration of candesartan on echocardiographic parameters in vivo. **(A):** Representative trace of M-mode echocardiogram from Sham-operated nude rats, control myocardial infarction (MI) (CNT), MI with BM-MSCs transplantation (BM), candesartan-pretreated BM (A-BM), and oral administration of candesartan after the transplantation (CNT+A, BM+A, A-BM+A) is shown. Changes in left ventricular ejection fraction (LVEF) from 2 to 4 weeks (**B**; ΔLVEF), LV end-diastolic dimension (**C**; ΔLVEDD), and LV end-systolic dimension (**D**; ΔLVESD) are averaged and shown. **(E):** Calculated LVEF from each group at 2 weeks after first operation are shown. There was no statistical significance; however, the degree of percentage EF tends to be worse in the oral administration series (right columns separated by dotted bar). Candesartan-pretreated BM significantly improved LVESD, consequently improved LVEF. *$p<0.05$. Abbreviations: BM, bone marrow; CNT, control; LVEDD, left ventricular end-diastolic dimension; LVEF, left ventricular ejection fraction; LVESD, left ventricular end-systolic dimension.

groups; on the other hand, change in LVESD (ΔLVESD) was significantly improved in A-BM group (vs. BM group) and A-BM+A group (vs. BM+A group), suggesting transplantation of candesartan-pretreated BM-MSCs significantly improved systolic function. Other echocardiographic parameter did not differ among the groups. There was no difference in the changes in body weight, serum BNP concentration, heart weight, LV systolic pressure, or LV end-diastolic pressure among the groups (Fig. 4). LV dP/dt was significantly improved by candesartan-pretreatment (A-BM vs. BM) with BM-MSCs; however, there was no additional effect of candesartan-pretreatment in the group of candesartan oral administration group (N.S. CNT-A vs. A-BM+A).

In this study, the beneficial effect was observed even in the ARB-pretreated BM-MSC transplantation group. The effect of ARB is known to cause an irreversible biological change in the cell, the "so-called" memory effect; therefore, such memory effect might affect cardiac function in vivo. To check this possibility, we cultured three groups of BM-MSCs: cells with candesartan for 2 weeks (ARB), cells without candesartan (CNT), and cells with candesartan for 1 week followed by 1 week without candesartan (1 week-ARB: washout for 1 week). The GeneChip analysis was performed among them, then the hierarchical clustering was used using the average distance method [20]. The gene expression pattern of 1 week-ARB was similar to CNT; therefore, the effect of ARB on BM-MSCs was reversible from the aspect of gene-chip analysis.

Incidence of Myocardial Transdifferentiation of ARB-Pretreated BM-MSCs In Vivo

To evaluate myocardial transdifferentiation of BM-MSCs in vivo, immunohistochemical analysis was performed. Antibodies against cardiac troponin-I (Trop-I) and connexin 43 were used. Confocal laser microscopic images could not detect EGFP-positive cardiomyocytes having clear striation staining pattern of Trop-I in the BM group. Sometimes enucleated EGFP-positive fragments of the cell at the center of the MI zone were observed, but taking the number of the injected EGFP-positive cells into account, the incidence seemed to be rare, as was reported previously [6, 19]. On the other hand, EGFP-positive and Trop-I double positive cells with clear striation staining pattern were observed at the marginal zone of the MI area in the candesartan-pretreated BM-MSC transplanted group (A-BM, Fig. 5F–5I). The oral

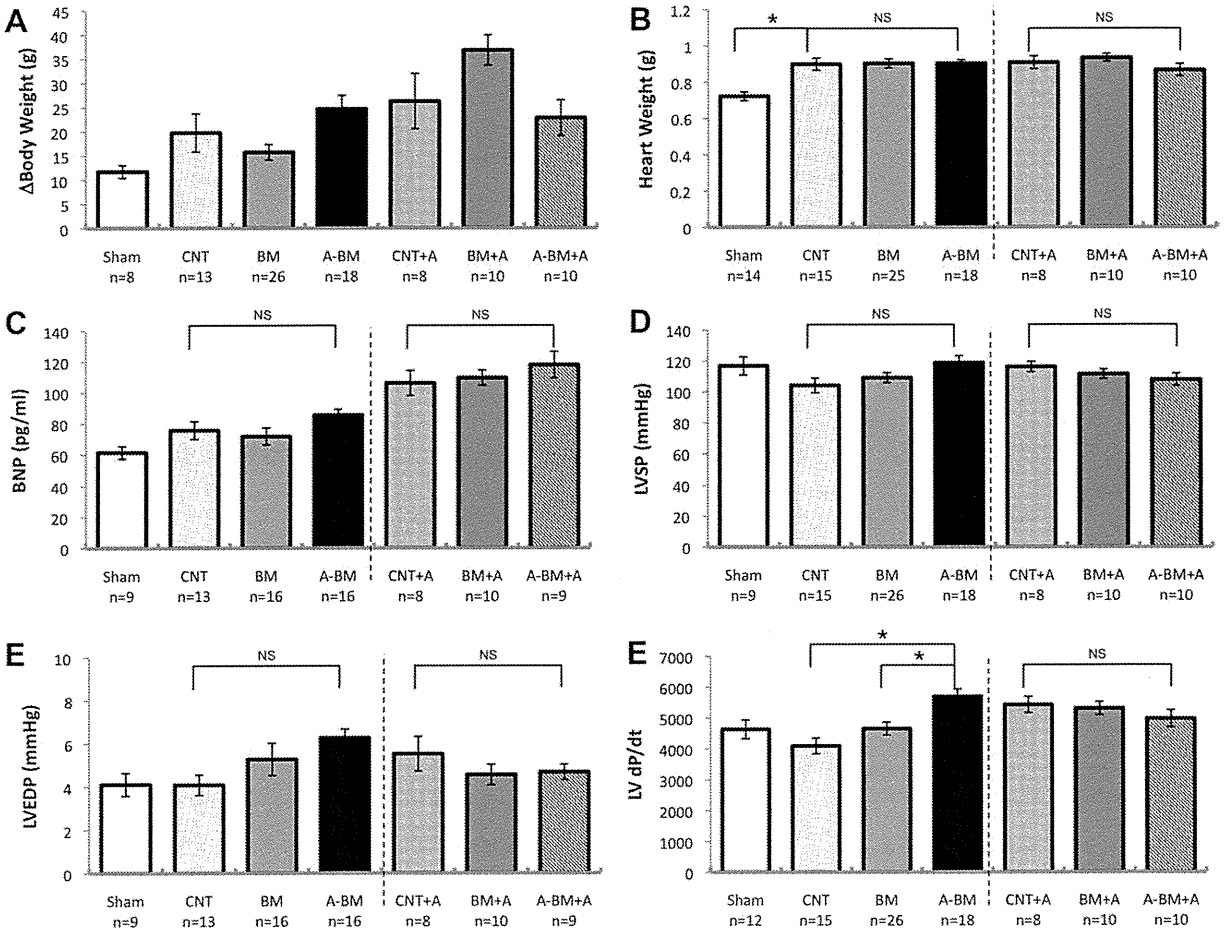

Figure 4. Effect of candesartan-pretreated bone marrow-derived mesenchymal stem cell (BM-MSC) transplantation and/or oral administration of candesartan on body weight, serum BNP concentration, and hemodynamic parameters. There was no difference in **(A)** changes in body weight, **(B)** heart weight, **(C)** BNP concentration, **(D)** left ventricular (LV) end-systolic pressure, or **(E)** end-diastolic pressure. **(D):** Effect of BM-MSCs on LV positive dP/dt is significantly improved by pretreatment with pioglitazone. **(F):** The LV dP/dt was significantly improved by transplantation of candesartan-pretreated BM-MSC (A-BM). *p<0.05. Abbreviations: BM, bone marrow; BNP, brain natriuretic peptide; CNT, control MI; LV, left ventricle; LVEDP, left ventricular end- pressure; LVSP, left ventricular systolic pressure.

administration of candesartan increased the incidence of survival of the EGFP/Trop-I double positive cells in vivo (A-BM+A, Fig. 5A–5E, 5J).

Genesis of Angiogenic Humoral Factors Derived from BM-MSCs by ARB

Angiogenic humoral factors were detected in the supernatant of the culture medium of BM-MSCs, suggesting that they are secreted from BM-MSCs, as reported previously [19]. However, the administration of 3 μmol/l of candesartan did not significantly affect the concentration of these angiogenic factors (Fig. 6). On the other hand, the angiogenic effect of candesartan-pretreated BM-MSCs was observed in vivo (Fig. 7A, 7B). In the peri-MI NZ, a CD34 positive area was not different among CNT, BM, and A-BM groups (without oral administration of candesartan). On the other hand, in the MI area, a CD34 positive area was significantly higher in A-BM group (vs. BM group). Oral administration of candesartan, significantly increased the CD34 area (CNT+A vs. CNT) in the peri-MI normal area and significantly increased it in the MI area. Masson trichrome staining and calculated MI volume at 2 weeks after transplantation (Fig. 7C, 7D) showed significant reduction of MI volume by pretreatment with candesartan of engrafted BM-MSCs (BM vs. A-BM) and the effect of pretreatment was not significantly augmented by the oral administration of candesartan.

Discussion

The Effect of Pretreatment with ARB in Human Neonatal BM-MSCs

The ARB did not affect the morphology of BM-MSCs and did not increase secretion of angiogenic humoral factors from BM-MSCs. The pretreatment with ARB significantly increased the CTE in vitro and in vivo. As pretreatment with ARB was essential for the effect on CTE, we concluded that the effect of ARB is not mediated by murine cultured myocardium, but directly affects BM-MSCs themselves, modifying the character of BM-MSCs. As the effect was not mediated by PD123319 as a selective AT2R blocker, the effect of ARB was mediated by the blockade of AT1R. In our previous article [19], activation of PPAR-γ significantly increased the CTE in BM-MSCs and the effect was completely blocked by GW9662, as a specific blocker of PPAR-γ receptor. The effect of telmisartan, which is known to have the strongest PPAR-γ activation activity among the ARBs, on CTE was partially blocked by GW9662, suggesting that the effect of ARBs is not mediated by PPAR-γ receptor activation activity. The

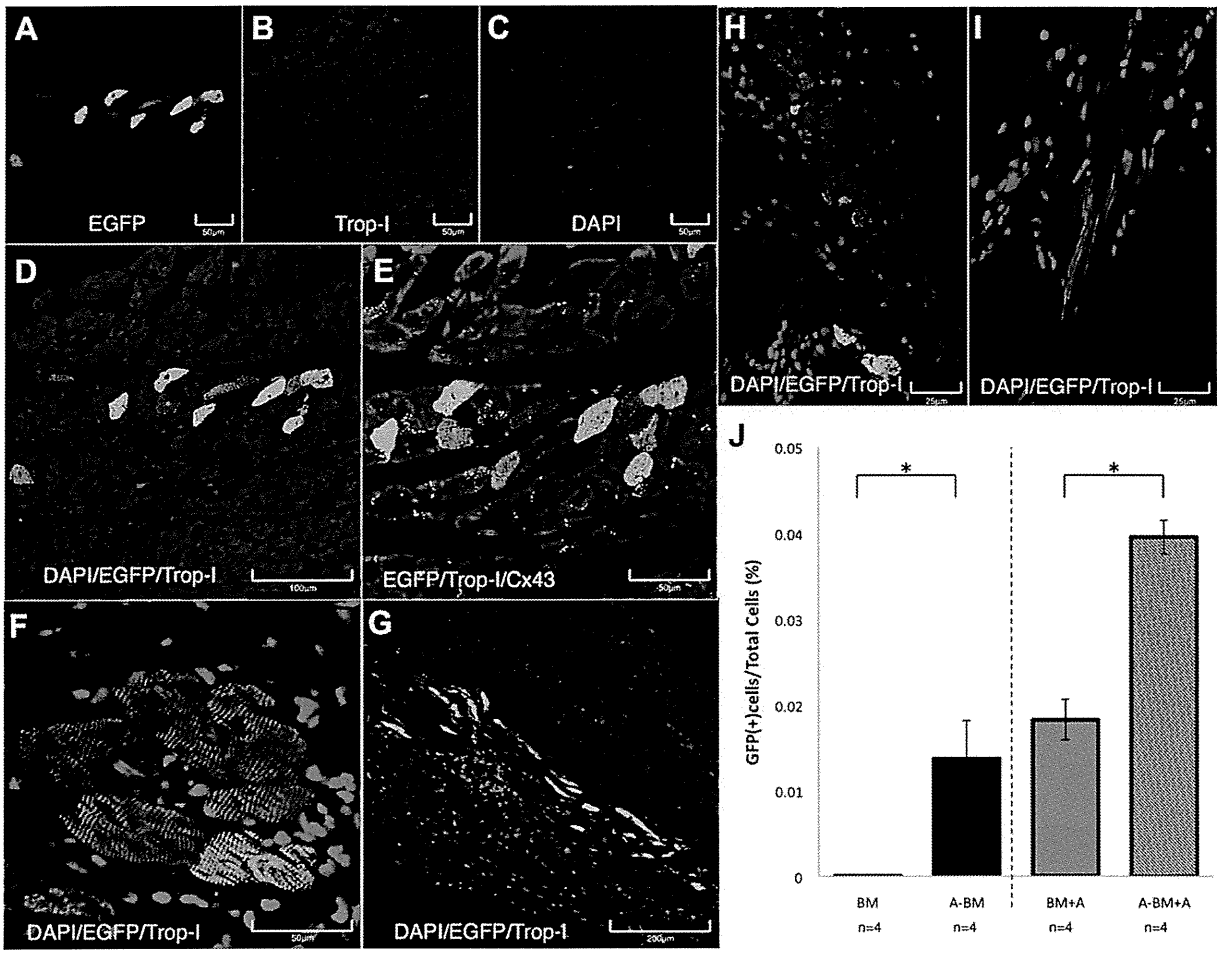

Figure 5. Both pretreatment and oral administration of candesartan significantly improved the incidence of survival of bone marrow-derived mesenchymal stem cell (BM-MSC)-derived cardiomyocytes in vivo. Confocal laser microscopic image of immunohistochemistry using anti-cardiac troponin-I antibody (red; Trop-I) is shown. **(A–C):** Lower magnification view for enhanced green fluorescent protein (EGFP) (green; **A**), Trop-I **(B)**, and 4′-6-diamidino-2-phenylindole (Blue; **E**) is shown. After transplantation of candesartan-pretreated BM-MSCs in the presence of oral administration of candesartan (A-BM+A), EGFP-positive cells can be observed at the margin of the myocardial infarction (MI), but there were many EGFP/Trop-I double positive cardiomyocytes survived at the peri-MI zone **(A)**. **(D):** Higher magnification view of merged image is shown. **(E):** The Trop-I positive cells are surrounded by dot-like staining of connexin 43 (white; Cx43). **(F):** Higher magnification view clearly shows striation staining pattern of Trop-I in the EGFP-positive cells. **(G):** At the center of MI zone (A-BM group), many EGFP-positive cells were enucleated and were negative for Trop-I. **(H, I):** However, there were some EGFP, Trop-I double positive rod-shaped cells at the center of MI zone. **(J):** The percentage of EGFP/Trop-I double positive cells in the injected EGFP-positive cells was averaged and is shown. By pretreatement with candesartan, the rate was significantly improved (A-BM vs. BM), and oral administration of candesartan additionally improved the incidence of EGFP/Trop-I double positive cells in vivo. Scale bars = 50 μm **(A–C, E, F)**, = 100 μm **(D)**, = 200 μm **(G)**, and = 25 μm **(H, I)**, respectively. *$p<0.05$. Abbreviations: BM, bone marrow; DAPI, 4′-6-diamidino-2-phenylindole; EGFP, enhanced green fluorescent protein; GFP, green fluorescent protein; Trop-I, troponin-I.

molecular mechanism of the effect of ARBs on CTE is still unclear. Further experiments should be done.

In the absence of valsartan as an AT1R selective blocker, administration of AT did not affect CTE; however, in the presence of valsartan, AT significantly increased CTE, suggesting that the relative stimulation of AT2R increased CTE. Furthermore, AT in culture medium seems to be generated by ACE activity in BM-MSCs, as the administration of ACE inhibitor to the BM-MSCs in culture significantly increased CTE in vitro. Furthermore, aliskiren did not affect the CTE; therefore, rennin and angiotensinogen did not play a role, but the angiotensin-I in the culture medium or autocrine from BM-MSCs must be a major source for AT.

Mechanism of Improving Systolic Function with ARB

Although EGFP-positive cardiomyocytes were observed in the candesartan-treated BM-MSC transplanted group, the number of them seems to be low for causing improvement in systolic function in vivo, as was seen in this study.

Concordant with the previous in vivo study [8] and clinical study [14], in the absence of BM-MSC transplantation, oral administration of candesartan suppressed the post-MI LV remodeling and progressive worsening of LVEF (CNT vs. CNT+A) at 2 weeks after MI. Furthermore, in this study, even in the absence of oral administration, the beneficial effect was observed in the candesartan-pretreated BM-MSC transplantation group. In this study, the effect of default BM-MSC transplantation was modest and there was no statistical significance from the control MI group. These data suggest that the ARBs modify the biology of BM-MSC, which play an important role in suppressing post-MI LV remodeling. This trend was observed in hemodynamic parameters and histological data. Pretreatment with candesartan significantly improved the efficacy of BM-MSC transplantation in augmentation of LV dP/dt and reduction in MI volume. Such

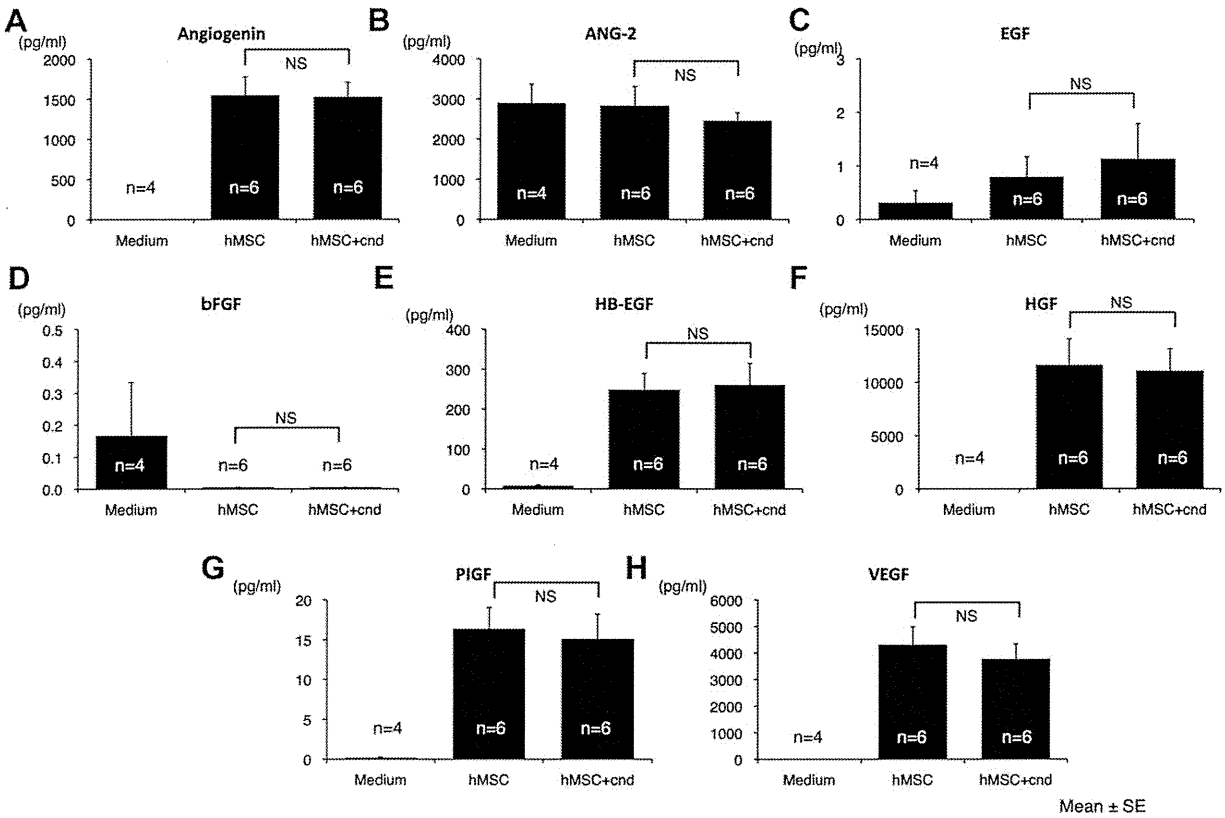

Figure 6. Secretion of angiogenic humoral factors from bone marrow-derived mesenchymal stem cells (BM-MSCs) into the culture medium supernatant and the effect of candesartan in vitro. Concentration of angiogenic humoral factors in **(A)** angiogenin, **(B)** angiotensin-2 (ANG-2), **(C)** epidermal growth factor (EGF), **(D)** basic fibroblast growth factor, **(E)** heparin-binding EGF-like growth factor, **(F)** hepatocyte growth factor, **(G)** phosphatidylinositol-glycan biosynthesis class F protein, and **(H)** vascular endothelial growth factor in culture medium was measured by enzyme-linked immunosorbent assay and averaged. Candesartan (cnd) treatment did not cause any significant change in angiogenic humoral factors secretion from BM-MSCs into the culture medium. Abbreviations: ANG-2, angiotensin-2; bFGF, basic fibroblast growth factor; cnd, candesartan; EGF, epidermal growth factor; HB-EGF, heparin-binding EGF-like growth factor; HGF, hepatocyte growth factor; hMSC, human mesenchymal stem cell; PIGF, phosphatidylinositol-glycan biosynthesis class F protein; VEGF, vascular endothelial growth factor.

cardioprotective effect of ARB-pretreated BM-MSCs may be due to augmentation of angiogenic effect and/or anti-apoptotic paracrine effect of BM-MSCs by pretreatment with ARB. The beneficial effect of ARB-pretreated BM-MSCs was also reported in the ischemia-reperfusion brain injury model [17], in which it was pointed out that both the stimulation of AT2R and blockade of AT1R have a significant effect on reducing brain damage in vivo and this data well correlated with our CTE data in vitro. In this study, the effect can be observed even by BM-MSC transplantation at 2 weeks after MI; therefore, the BM-MSC-induced angiogenesis might have suppressed ongoing post-MI LV remodeling. In this study, there was discrepancy between the angiogenic effect of ARB-pretreatment in BM-MSCs in vitro and in vivo. We speculated that additional angiogenic effect of BM-MSC transplantation by ARB-pretreatment might require graft-host interaction, that is, immunological reaction or inflammation in the host myocardium.

Cell Fusion-Independent Cardiomyogenic Transdifferentiation

Extensive evidence of cell fusion-independent cardiomyogenic transdifferentiation of human MSCs was presented in our previous study [6, 9–11, 19]. In this study, the incidence of cell fusion was approximately 1% and it was not affected by ARB pretreatment; therefore, the increase in EGFP-positive cardiomyocytes by ARB treatment was due to an increase in efficiency of cardiomyogenic transdifferentiation in vitro. Furthermore, there were no EGFP/Trop-I double positive rod shaped cardiomyocytes in the default BM-MSC transplanted group; on the other hand, the appearance of significant numbers of EGFP/Trop-I double positive cardiomyocytes was observed in ARB-pretreated BM-MSC transplanted group. This suggests an improvement of CTE of BM-MSCs in vivo by ARB pretreatment. Taking into account our previous study and our present in vitro experiment, we concluded that our observed EGFP/Trop-I double positive cells in vivo are caused by cardiomyogenic transdifferentiation.

Clinical Application

The efficacy of human BM-MSC transplantation had been modest [14, 15], and a new method for BM-MSC transplantation that will gain dramatic improvement in efficacy is expected. Genetic modification, that is, over-expression of the *AKT*-gene was reported to improve efficacy of BM-MSC transplantation in vivo [21]; however, use of such genetically modified cells raises a safety concern, that is, tumorgenecity. In comparison with the genetic modification, modification of BM-MSCs by ARBs, which are commonly used for heart failure patients, is a method that is ready to use for clinical patients.

In addition to the beneficial efficacy for cardiac function, this experimental model may also give us a clue to improving CTE in vivo, which is very essential for cardiac regenerative therapy. The precise mechanism for cardiomyogenic transdifferentiation of human BM-MSCs has been unclear. As the

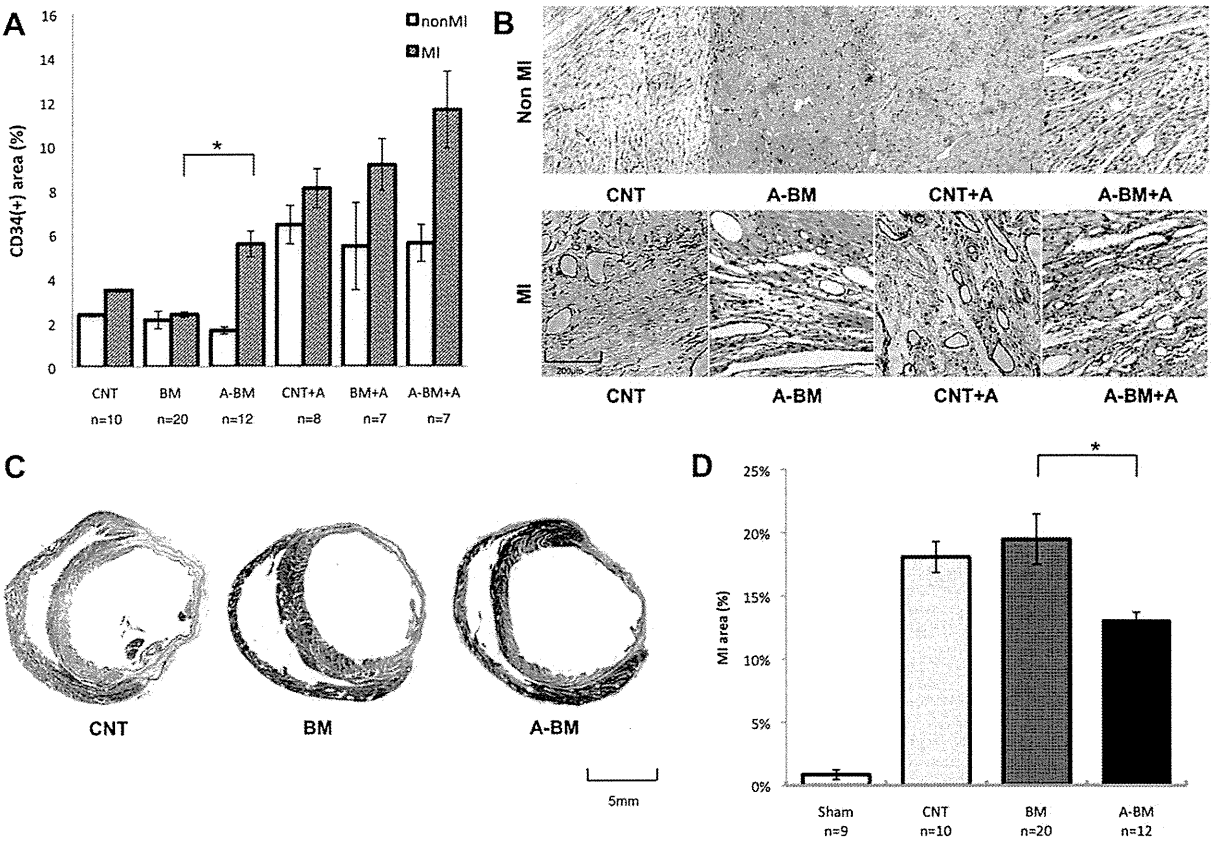

Figure 7. Effect of bone marrow-derived mesenchymal stem cell (BM-MSC) transplantation and/or treatment with candesartan on vessel density and infarction size in the heart in vivo. **(A):** The percentage of CD34 positive area in control myocardial infarction (MI) (CNT), MI with bone candesartan-pretreated BM-MSCs transplantation (BM), candesartan-pretreated BM (A-BM), and additional oral administration of candesartan after the transplantation (CNT+A, BM+A, A-BM+A) are calculated and averaged. **(B):** Representative microscopic image of immunohistochemistry using anti-CD34 antibody to detect vessels at center of MI zone and peri-MI normal zone (non-MI) are shown. Scale bar = 20 μm. Pretreatment with candesartan significantly increased vessel density at MI zone; on the other hand, oral administration of candesartan significantly increased vessel density at non-MI zone. **(C):** Representative masson-trichrom staining of the heart at the tendinous cord level of CNT, BM, and A-BM are shown. The digitized data were measured and calculated in **(D)**. By the candesartan-pretreatment, BM-MSC transplantation significantly decreased in percentage fibrosis volume. Scale bar = 5 mm. *p<0.05. Abbreviations: BM, bone marrow; CNT, control; MI, myocardial infarction.

incidence of cardiomyogenic transdifferentiation of human BM-MSCs is extremely rare, it has been impossible to statistically analyze the effect on CTE of various drugs or interventions in vivo. Therefore, there has been no systematic strategy for improvement of CTE of BM-MSCs until our previous article [6, 9–11, 19]. Our in vivo model of ARB-treated BM-MSCs is able to statistically analyze the effects of drugs on CTE, which is important for further improvement of CTE. In vitro, the pioglitazone's effect on CTE was independent from the effect of ARB; therefore, the additional administration of pioglitazone, as a PPAR-γ activator may be expected to improve CTE further. Further experiments should be done.

Study Limitation

In our previous study, we have used BM-MSCs obtained from a 41-year-old and a 90-year-old men. The CTE results were 1% and 0.3% in vitro [19], respectively. In this study, the CTE of default BM-MSCs from neonates was approximately 3%–5%. This data implies BM-MSCs obtained from younger generations that may have higher cardiomyogenic transdifferentiation ability. As ARB is known to have a potential for an anti-aging effect, the effect of ARB on BM-MSCs might increase the CTE by ARB's anti-aging effect on BM-MSCs. Further experiments should be done on this issue.

In vivo MI model was performed by two series (Sham, CNT, BM, A-BM series and CNT-A, BM-A, A-BM-A series) at different periods. As it was difficult to control the size of the MI at the coronary ligation, the size of the MI of later series are slightly larger (N.S.) than the former series. Therefore, we did not perform statistical analysis on some parameters between the series (separated by dotted line in the figures). The serum BNP level and the size of percentage MI volume are slightly larger in the later series. In this study, intra-individual difference values were compared with the values of the two series.

Conclusion

Pretreatment with angiotensin receptor blockers (ARBs) in culture activate human marrow-derived mesenchymal stem cells by angiotensin-II receptor type 1 blockade. ARBs-pretreated human marrow-derived msenchymal stem cells was significantly improved cardiomyogenic transdifferentiation efficiency in vitro and in vivo, and transplantation of the ARBs-pretreated cells significantly improved cardiac function and can be a promising cardiac stem cell source from which to expect cardiomyogenesis.